UNIVERSIDAD DE CONCEPCIÓN

FACULTAD DE INGENIERÍA

DEPARTAMENTO DE INGENIERÍA METALÚRGICA

EXPERIMENTAL STUDY OF ORE FLOW TO ASSESS THE FEASIBILITY OF USING LONG ORE PASSES FOR THE DECARBONIZATION OF HAULING IN DEEP MINING OPERATIONS

POR

Fernanda Scarlet Vera Valverde

Memoria de Título presentada a la Facultad de Ingeniería de la Universidad de Concepción para optar al título profesional de Ingeniera Civil de Minas

Profesor Guía
Dr. Rene Gómez Puigpinos

Profesional Supervisor
Dr. Ebrahim Fathi Salmi

Octubre 2024
Concepción (Chile)

Dedicatoria

A mi familia, por ser el fundamento de todo lo que soy y hago. Su amor y apoyo incondicional me han dado la fortaleza para superar cualquier obstáculo. A mis padres, en particular, les agradezco profundamente por su amor y sacrificio a lo largo de mi vida, por enseñarme el valor del esfuerzo y la perseverancia, y por estar siempre a mi lado en cada paso que doy.

A mis hermanos y hermanas en la Tierra y en el cielo, por ser mis compañeros de vida, sus palabras de aliento y por brindarme momentos de alegría y apoyo en cada etapa que avanzamos juntos.

A mis amigos y amigas, por su leal compañía, por las risas compartidas, por los buenos y malos momentos que pasamos juntos, y por ofrecerme su apoyo y consejos cuando lo necesité.

A mi pololo, por su amor y apoyo inquebrantable. Gracias por ser mi compañero, regalarme tu alegría, por creer en mí en cada decisión y siempre estar presente.

A mis profesores de la universidad, por su guía, conocimientos y dedicación, los cuales fueron esenciales para mi crecimiento académico y personal.

Gracias a todos por ayudarme a crecer, ser mejor persona y profesional cada día, por ayudarme a construir quien soy y quien quiero ser. Y gracias a la vida, por darme tanto.

Agradecimientos

Quiero expresar mi más sincero agradecimiento a CSIRO Australia por brindarme la oportunidad de colaborar en este proyecto, y realizar mi memoria de título y práctica profesional junto a ellos. También, me siento profundamente agradecida con la Universidad de Concepción y el Departamento de Ingeniería Metalúrgica por su respaldo y asistencia durante este proceso.

Me gustaría expresar un agradecimiento muy especial a mis tutores, el Dr. Ebrahim Fathi Salmi y el Dr. René Gómez, quienes fueron una guía esencial a lo largo de este proyecto. Siempre estuvieron dispuestos a ofrecer su ayuda y compartir su conocimiento de manera generosa. Su dedicación, paciencia y orientación fueron fundamentales para el éxito de este trabajo. Su apoyo constante no solo enriqueció mi investigación, sino que también me brindó la confianza necesaria para superar cada desafío que enfrenté.

Igualmente, agradezco a la Dra. Constanza Paredes y al Dr. Ewan Sellers, quienes sin conocerme confiaron en mi, y me ayudaron a obtener esta maravillosa oportunidad. Su guía, consejos y sabiduría han sido invaluables en esta travesía.

Sin duda tuve el mejor team.

Resumen

La disminución continua en la ley de los minerales ha obligado a la industria minera a implementar nuevas estrategias para mantener e incluso aumentar la producción, especialmente debido a la creciente demanda de minerales estratégicos y críticos como el cobre, que es crucial para la transición energética. El cobre extraído de minas subterráneas mediante métodos de hundimiento frecuentemente emplea piques de traspaso, como un método de transporte del mineral entre niveles. El aumento en el uso y extensión de los piques de traspaso en la producción minera tiene el potencial de mejorar la eficiencia, reducir el consumo de energía y disminuir las emisiones de carbono, específicamente en el transporte de materiales. Sin embargo, existen desafíos significativos relacionados con el flujo gravitacional en los piques de traspaso debido a las grandes distancias verticales en estos métodos y a la mayor profundidad de las actividades mineras.

Para abordar estos desafíos, este estudio emplea un modelo físico a escala para examinar las características del flujo de diferentes tipos de partículas dentro de un pique de traspaso. Las variables analizadas incluyen diferentes porcentajes de llenado, distribuciones de tamaño de partículas y propiedades de las partículas. Se realizaron un total de 4160 experimentos de flujo, utilizando 52 combinaciones de formas y tamaños de partículas, para identificar y cuantificar el efecto de diferentes variables en el flujo del material.

En los resultados experimentales, el mayor número de colgaduras se registró para partículas prismáticas triangulares grandes, con un total de 125 atascos, seguidas por partículas esféricas grandes, con 96 atascos. En contraste, no se observaron atascos en experimentos con partículas esféricas pequeñas y partículas octaédricas. Además, el índice de frecuencia de atascos se reduce en un 98.48% cuando la esfericidad disminuye en un 23.47%. Esto indica que una disminución en la esfericidad tiene un impacto significativo en el flujo de partículas. En partículas esféricas, menores niveles de llenado del pique de traspaso reducen el número de atascos; sin embargo, en partículas de forma prismática mixta, este efecto no se observó.

El análisis detallado de los eventos de atascos bajo diversas condiciones ayuda a identificar escenarios críticos de flujo de partículas dentro de los piques de traspaso. Los hallazgos proporcionan información invaluable sobre las condiciones críticas que afectan el flujo de partículas, mejorando así nuestra comprensión de la dinámica compleja en las operaciones de los piques de traspaso de mineral.

Table of Content

List of Figures

List of Tables

This study is presented through a paper submitted to an international journal (IJRMMS).

Experimental study of ore flow to assess the feasibility of using long ore passes for the decarbonization of hauling in deep mining operations.

Javiera Brevis[1,2], Fernanda Vera[1,2*], René Gómez[2], Ebrahim F. Salmi[1]

1. Sustainable Mining Technologies, CSIRO, Pullenvale, Australia, 4069

2. Universidad de Concepción, Chile

***Correspondent Author:** fernanda.veravalverde@csiro.au

Abstract

The continuous decline in ore grades has compelled the mining industry to implement new strategies to maintain and even increase production, especially due to the growing demand for strategic and critical minerals such as copper, which is crucial for the energy transition. Copper extracted from underground mines using caving methods frequently employs ore passes as a method of transporting ore between levels. The increased use and extension of ore passes in mining production has the potential to enhance efficiency, reduce energy consumption, and lower carbon emissions, specifically in hauling. However, there are significant challenges related to gravitational flow in ore passes due to the significant vertical distances in these methods and the increased depth of mining activities. To address these challenges, this study employs a scaled physical model to examine the flow characteristics of different particle types within an ore pass. Variables analysed include different filling percentages, particle size distributions, and particle properties. A total of 4160 flow experiments were performed, using 52 combinations of particle shapes and sizes, to identify and quantify the effect of different variables on the flow of the material. The highest number of hang-ups was recorded for large triangular prismatic particles, with a total of 125 hang-ups followed by large spherical particles, with 96 hang-ups. In contrast, no hang-ups were observed in experiments with small spherical particles and octahedral particles. Additionally, hang-up frequency index is reduced by 98.48% when sphericity decreases by 23.47%. This indicates that decreasing sphericity has a significant impact on particle flow. In spherical particles, lower ore pass filling levels reduce the number of hang-ups nevertheless, in mixed prismatic shape particles this effect was not observed. The detailed analysis of hang-up events under various conditions aids in the identification of critical particle flow scenarios within ore passes. The findings provide invaluable insights into the critical conditions affecting particle flow, thereby enhancing our understanding of the complex dynamics at play in ore pass operations.

Key words: Ore passes, flowability, hang-up frequency index, physical modelling, particle shapes, particles sizes

1. Introduction

The incorporation of ore pass systems is an attractive low-operational-cost alternative, especially at greater depths, to improve material handling strategy in underground mining. However, to achieve optimal performance of these systems, good flowability is crucial [5, 8, 52]. If critical variables (e.g., material properties, geometry, overload) are not favorable, interruptions in material flow can occur. The most common event interrupting the flow in an ore pass, which also has the potential to cause accidents within the mine, is hang-ups [27]. Hang-up occurrence implies operational downtime and often complex hang-up reduce manoeuvres [28, 62]. Various studies on simulating material flow within an ore pass have employed a range of methods, including physical models, numerical models, and mine databases. These approaches have contributed to the development of empirical design rules and recommendations to prevent flow interferences. Physical models are widely used due to their ability to offer controlled experiments [4, 14, 16, 25]. Conversely, numerical models also play a crucial role in these studies, though they tend to provide more conservative results [27, 46, 54, 64]. A significant challenge with numerical models is that some ignore the shape of the particles flowing within the ore pass, despite evidence that this critically affects material flowability and particle interactions and the probability of interlocking. Nevertheless, conclusions from numerical models are often corroborated with physical experiments. Moreover, mine databases have been used for design studies, providing valuable information and validating conclusions from the other methods [22, 26, 43].

In general, studies evaluating the implementation of ore passes confirm that productivity could be increased, provided discharge time remains low. This implies that flowability issues in the ore pass must be avoided to ensure efficient operation [39] A critical aspect of ore pass operation is also understanding potential failure modes, which usually depend on strategies developed from feasibility through to design and operation stages [31, 59]. Inadequate decisions, such as locating an ore pass in poorly characterised waste rock to optimise ore recovery, or locating the ore pass in an area that will be affected by the dynamic mining stresses can compromise the stability of the ore pass and endanger its integrity, potentially leading to accidents [53]. However, failures can also arise from other causes, and their nature varies depending on the specific type of host rocks. Literature provides several examples of ore passes encountering issues such as localised or large-scale collapses, strain bursts, squeezing layers, creeping rocks, faulted and tectonized zones, and brecciated grounds that lead to unravelling [7, 18, 21, 32, 38, 57, 68]

Several failure modes in an ore pass can affect its operation. Spalling-induced failure, which is known as dog-ears, occurs due to wall deformation from cross-sectional convergence, leading to block detachment and embedment in the walls [39] Air and dust blasts happen when ore falls and disperses dust around the area [39] Abrasive wall wear is caused by the flow of coarse material, increasing the ore pass diameter. Mud rushes also occur under specific conditions, such as the presence of water and fine material [9, 39]. Structural failures result from adverse geotechnical conditions, inadequate design, improper excavation methods, erosion, the presence of water, dynamic loads, and poor maintenance [29]. The most common failures are hang-ups, involving flow interferences that can occur along any length of the ore pass [60] and are dangerous due to the sudden release of material during hang-up removal [4]. These hang-ups are categorised into three types: interlocking hang-ups, where large rocks interlock in a stable pattern [34, 35], cohesive hang-ups, caused by the accumulation of cohesive material from clayey, fine material and water mixtures [33, 63], and foreign material, where the poor condition of the ore pass lining or support interacts with the ore flow, causing hang-ups [3, 7]. There have also been occasional instances in cold regions where hang-ups occur primarily due to the freezing of wet ore within ore passes [37, 55]. While this may not be an issue in regions like Australia or Africa, it has posed challenges in areas such as Canada, Kazakhstan, Russia, Mongolia, Sweden, and mountainous regions in Chile. There is no universal rule for determining the appropriate dimensions of an ore pass, so empirical methods based on scaled physical models and simulations are generally used for sizing [33, 46, 49, 64]. For the ore pass diameter, a minimum ratio between the ore pass dimension (D) and particle size (d) is recommended to avoid hang-ups, ensuring that the ore size is sufficiently small compared to the diameter. Generally, an opening at least 5 to 6 times larger than the largest particle is accepted as sufficient to prevent hang-ups [33, 42, 53]. While the design could be limited to selecting the larger ratio, it is also necessary to consider that a smaller ore pass diameter is more stable, cheaper to implement, and creates less disturbance in the surrounding host rock, whereas a larger diameter is more expensive to excavate and increases rock support demands [39]. In the past, controlling the maximum allowable entry size into the ore pass was done through unreliable methods based on the operator's visual selection. Currently, the installation of bars in the loading area, such as scrapers, grizzly, and mantle, helps control the ore size distribution entering the ore pass [3, 33], restricting coarse material entry and reducing interlocking hang-up probabilities.

The ore pass length depends on the distance between levels or transport infrastructure, operational needs, technical limitations, and mine design [37] Currently, there are increasing cases of long ore passes of 300 to 500 m and ultra-long (over 500 m), in some cases extending up to approximately 650 m [50]. The ore pass inclination should be determined based on material characteristics [18] and the need to reduce impact forces [19, 20]. However, a less vertical inclination may not provide the necessary material flow [6, 40] and complicate hang-up removal [28, 62]. Methodologies based on design charts relating ore pass inclination to flow efficiency or mobility are available, allowing optimization for different material types [34, 35]. Some of these charts also include additional operational and design aspects, useful for comprehensive ore pass planning. However, it is essential to consider other factors such as geotechnical conditions, load capacity, and excavation methods to ensure effective and safe design [3, 33].

Another design aspect to consider is the shape of ore passes. Various configurations exist regarding ore pass shapes, with circular and square being the most common. The choice depends on several factors, including the type of material to be transported, site geotechnical conditions, construction ease, material flow efficiency, and long-term stability and durability. Square sections can improve the flow of cubic rock fragments compared to circular sections [27]. Conversely, circular sections are preferred in high-stress environments due to their greater structural stability [28]. It is also noted that when the length of ore passes approaches or exceeds 100 m, the most efficient and practical method for their implementation is raise boring, which results in ore passes with a circular cross-section. Additionally, ore pass reinforcement with different forms of abrasion resistance linear is often used to enhance stability and longevity [30, 68]. This lining can affect material flow by altering roughness, reducing friction between the material and ore pass wall [31, 67], reducing the risk of impact-induced damage and wall unevenness and facilitating smoother material flow [67]. Without lining, roughness depends on the excavation method, damage due to impact-induced damage, and natural characteristics of the rock mass [65, 66]. However, ore flow often removes asperities of the wall surfaces and smoothens the wall regardless of the excavation method [27].

On the other hand, the extraction rate can also mitigate hang-ups, preferably using continuous flow by extracting ore from the passes at least once during each work shift [6, 63], preventing material consolidation inside the passes. However, constant ore flow increases the interaction between ore and walls can cause ore pass damage due to abrasion [7, 67]. Additional elements such as chutes and gates can help maintain controlled extraction, reducing material speed during withdrawal and controlling dust movement [60]. Gates are useful when there is a need to limit material flow in a long ore pass, such as the junction of different production levels and rise fingers [39].

The characteristics of the material transported in ore passes, such as strength, friction, cohesion, and shape, are difficult to control and have a significant impact on the flowability of ore [40, 41, 61]. Other variables, such as the presence of water, can alter the material's behaviour, affecting the viscosity of the ore and increasing or decreasing the risk of cohesive hang-ups and mud-rushes [13, 15, 47]. Additionally, confinement within the ore pass is difficult to control, and long distances travelled lead to increased fragmentation, which produces a greater amount of fines [22, 23], which, along with moisture, could favour the formation of cohesive hang-ups. Therefore, having good characterization is beneficial to help estimate the material flow behaviour within the ore pass.

Although various previous studies on flow in ore passes have helped to define some of the important design parameters and allowed the development of some guidelines, there are still variables that impact the phenomenon of ore pass flow dynamic that need to be studied and quantified, especially when considering the design of long ore passes. The limitations in the heterogeneity of the muck in terms of size and shape of the particles have not been deeply analysed. This is a key factor that will be investigated in this work to understand the functioning and behaviour of hang-ups considering various possible conditions.

2. Experimental methodology

Modelling hang-ups in ore flow is a complex task due to the multitude of variables involved. In this article, we focus on analysing how the use of a wide range of particle sizes and shapes affects the generation of hang-ups. Additionally, we examine how these effects vary based on different filling percentages of the passes. To achieve this, we employed a scaled physical model (Figure 1) that represents the material flowing within an ore pass.

The experiments were conducted in two stages. In the first stage, eight types of particles with different shapes and sizes were tested independently without mixing different particle types. In the second stage, the particles were mixed in different amounts, producing 44 unique combinations. In both stages, hang-ups were observed, and the mass extracted between the hang-ups were quantified, with this relationship defined as hang-up frequency index, *HFI,* as per [14, 47]. (see Eq. 1).

$$HFI \text{ (gram/hang-up)} = \text{Mass of ore extracted between hang-ups} \quad (1)$$

2.1 Physical Model

The simulation of particle flow within an ore pass was conducted using a small-scale physical model, utilising a single cylindrical acrylic tube (**¡Error! No se encuentra el origen de la referencia.**-c) with a diameter of 31 mm, a length of 780 mm, and a 90° inclination. Continuous extraction was performed through a single opening, matching the cylinder's diameter. The experimental model variants included the filling percentage based on the cylinder's total volume (100%, 75%, 50%, and 25%) and the type of particle used to represent the ore.

The physical model was constructed from acrylic to allow clear visibility of the material flow (**¡Error! No se encuentra el origen de la referencia.**), facilitating the recording of desirable parameters during the tests. The only disadvantage of acrylic is its low wall friction angle, which might deviate from real conditions. The stand was built with steel to prevent external movements that could affect flow behaviour, ensuring stability during extraction. No additional external loads were used, so the overburden was low, and fragmentation was null, considering only the weight of the particles within the ore pass. An example of a hang-up formed in the model is shown in Figure 1-b.

(a) (b) (c) (d)

Figure 1: The ore pass experimental model. a) A view of the simple rig, and b, c, d) Examples of hang-up observed during the flow of different muck types

The apparatus can also be modified to simulate the effects of changes in ore pass diameter, accounting for the impact of irregularities in ore pass geometry caused by localised collapses or wear and tear of the liner and surrounding rock due to impact-induced dynamic loads (see Figure 2).

Figure 2: View of the apparatus built at CSIRO to investigate the flowability of rock-like fragments in pipes

2.2 Muck Materials

In stage one of the research, eight cement particles with different sizes and shapes were used, and subsequently (in the second stage of experiment), 44 combinations based on the original eight particles were made. Table 1 shows reference photographs taken with a particle size and shape analyser (CAMSIZER X2).

Table 1: Particle name, diameter (d80) [mm] and shape, for the 8 original samples of particles.

Particles	S1	S2	S3	S4	I1	O1	P1	P2
				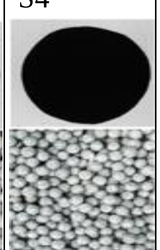				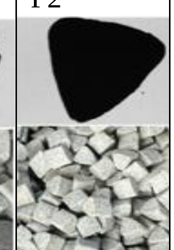
d80 [mm]	9.99	7.65	6.30	4.11	5.16	3.03	10.06	6.61

Ratio D/d	3.1	4.05	4.92	7.54	6.01	10.23	3.08	4.69

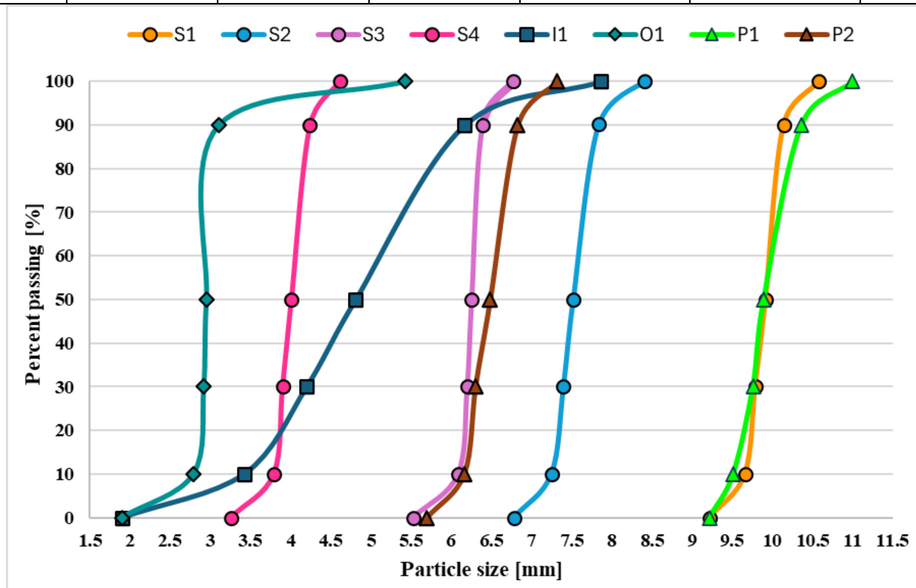

Figure 3: Granulometric curves, for the eight original muck types (S1, S2, S3, S4, I1, O1, P1 y P2).

Material characterisation was performed to obtain relevant information about the particles to be used. The particle-size-distributions were obtained using a particle size and shape analyser (CAMSIZER X2). This device was also used to measure the density, sphericity, roundness, symmetry, and convexity of the particles, with the maximum value being one for perfectly spherical particles. The definition of these parameters can be found in relevant literature [51], including the CAMSIZER X2 manual [45], and will therefore not be repeated here. From these data, additional parameters were derived, as shown in Table 2. Furthermore, other instruments were employed, such as a point load testing machine (INSTRON) to obtain the IS50, and an inclinometer to measure the friction between the wall and the particle. Note that the IS50 was measured to ensure particle strength and to prevent secondary fragmentation during flow, thereby maintaining the particle size distribution. In Figure 3, particle-size-distributions of the eight particles used in stage one are presented.

Table 2: Main material properties, for the 8 original particle samples.

Sample characteristics	**S1**	**S2**	**S3**	**S4**	**I1**	**O1**	**P1**	**P2**
Density [g/cm3]	5.93	7.54	7.98	8.36	23.38	10.17	5.88	7.71
Swell [%]	20	15.7	14.8	14.2	7.1	11.5	57	37
Uniformity coefficient [D60/D10]	1.04	1.06	1.04	1.12	1.8	1.11	1.09	1.11
Ratio D/d	3.1	4.05	4.92	7.54	6.01	10.23	3.08	4.69
Repose angle [°]	14.3	12.1	17.4	16	29.3	30.1	30.26	28.3
IS50 [Mpa]	18.8	15.7	19.7	25.6	3.8	7.8	14.1	13.2
Wall-sample friction [°]	3.89	3.97	3.16	2.04	26.2	23.28	30.98	20.71
Sphericity	0.98	0.98	0.98	0.96	0.75	0.78	0.8	0.85
Roughness	1	1	1	0.99	0.01	0	0	0.01
Simetry	0.99	0.99	0.99	0.99	0.87	0.9	0.91	0.91
Convexity	1	1	1	1	0.98	0.99	0.99	0.99

The material characterisation and size distribution performed will be utilised in the final stage of analysis to determine whether any correlation or trend predominates, based on the data recorded with the physical model, specifically with the hang-up frequency. The compositions of the particle mixed used in the second stage of experiments are shown in Figure 4. This figure displays the forty-four combinations made from the original eight particles and their respective percentages within the synthesised muck.

This step is crucial, as ore flowing through ore passes comprises particles of varying shapes and sizes. These characteristics often evolve during ore flow due to particle interactions, the impact of muck dumping, and contact with the walls. Consequently, ore passes can act similarly to crushers and mills, further reducing particle sizes and shapes [24, 25]. In comminution, the most stable rock fragment shape is spherical particles with size range between 25 mm to 150 mm known as critical sizes [56], leading to an expected increase in the sphericity of rocks passing through ore passes.

2.3 Experimental plan

The experiment was initiated to investigate the flow of different muck types by filling the tube with each particle sample independently based on the filling percentage (100%, 75%, 50%, and 25%). Extraction was then performed through an aperture located at the bottom of the model, which allowed for the opening and closing of the particle passage. For each flow experiment, twenty tests were conducted per filling level to ensure replicability. Extraction involved fully opening the gate and depending on the flowability of the muck materials, either all the material was extracted, or some remained in the tube. This procedure was repeated for all experiments, conducted in stages one and two of the research, resulting in data from 4160 tests. The experimental plan is outlined in Table 3.

Since the flowability of particles within an ore pass can be quantified based on the produced interferences, the parameters measured during each extraction included the mass after each interference (hang-up), the height of the interference, and the number of interferences.

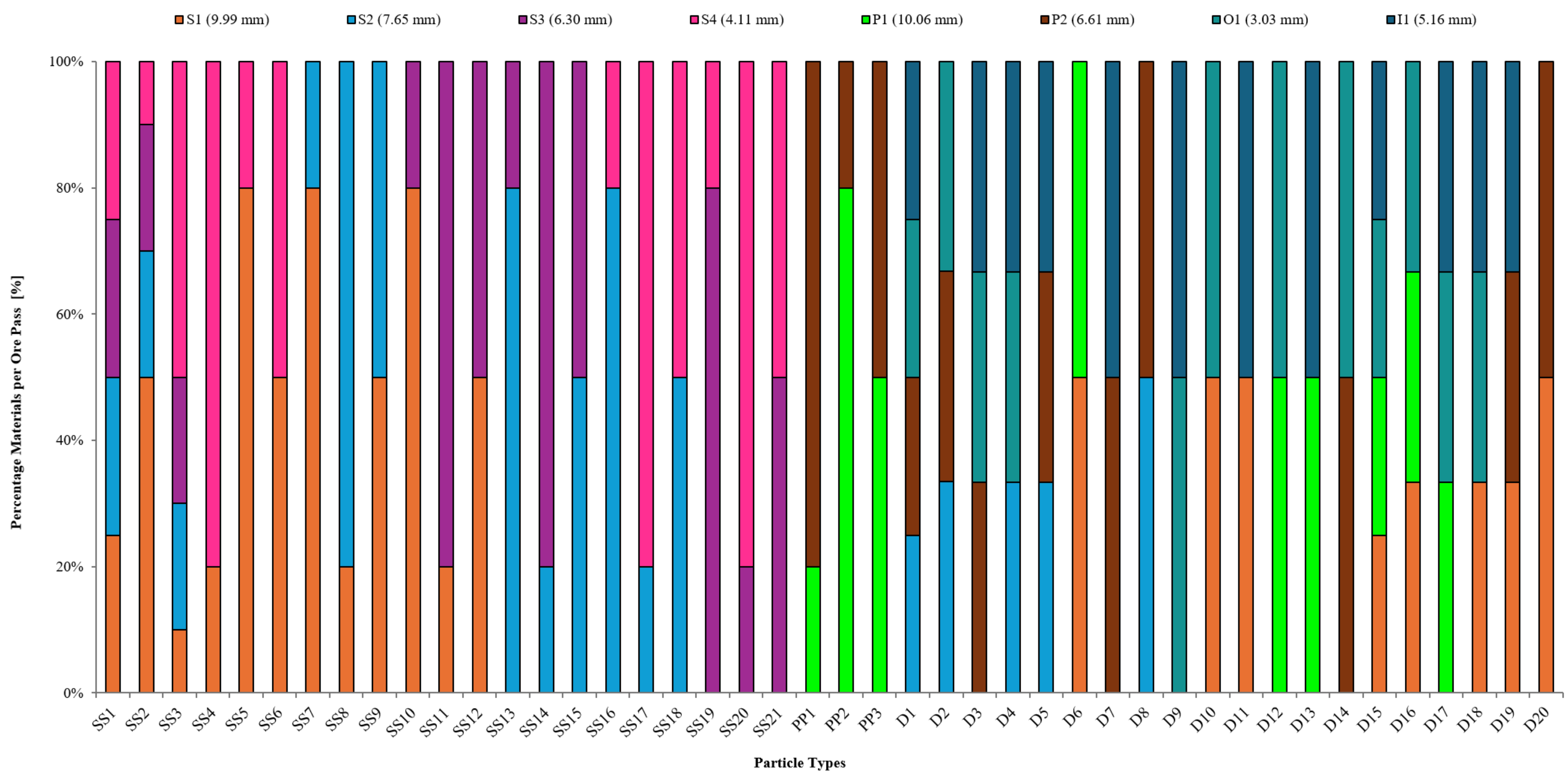

Figure 4: Particle type distribution, 44 combinations made with the original 8 particles (S1, S2, S3, S4, I1, O1, P1 y P2).

Table 3: Experimental plan, according to sample type and filling percentage

<table>
<tr><td>Stage</td><td colspan="8">Stage 1</td><td colspan="44">Stage 2</td></tr>
<tr><td>Type of sample</td><td colspan="8">Orginal particles</td><td colspan="20">All shapes combinations</td><td colspan="21">Sphere combinations</td><td colspan="3">Prism combinations</td></tr>
<tr><td>Name of sample</td><td>S1</td><td>S2</td><td>S3</td><td>S4</td><td>P1</td><td>P2</td><td>O1</td><td>I1</td><td>D1</td><td>D2</td><td>D3</td><td>D4</td><td>D5</td><td>D6</td><td>D7</td><td>D8</td><td>D9</td><td>D10</td><td>D11</td><td>D12</td><td>D13</td><td>D14</td><td>D15</td><td>D16</td><td>D17</td><td>D18</td><td>D19</td><td>D20</td><td>SS1</td><td>SS2</td><td>SS3</td><td>SS4</td><td>SS5</td><td>SS6</td><td>SS7</td><td>SS8</td><td>SS9</td><td>SS10</td><td>SS11</td><td>SS12</td><td>SS13</td><td>SS14</td><td>SS15</td><td>SS16</td><td>SS17</td><td>SS18</td><td>SS19</td><td>SS20</td><td>SS21</td><td>PP1</td><td>PP2</td><td>PP3</td></tr>
<tr><td>Fill level per sample</td><td colspan="2">100%</td><td colspan="2">75%</td><td colspan="2">50%</td><td colspan="2">25%</td><td colspan="11">100%</td><td colspan="11">75%</td><td colspan="11">50%</td><td colspan="11">25%</td></tr>
<tr><td>N° Experiments per sample</td><td colspan="2">20</td><td colspan="2">20</td><td colspan="2">20</td><td colspan="2">20</td><td colspan="11">20</td><td colspan="11">20</td><td colspan="11">20</td><td colspan="11">20</td></tr>
<tr><td>Total experiments per sample</td><td colspan="8">80</td><td colspan="44">80</td></tr>
<tr><td>Total experiments per step</td><td colspan="8">640</td><td colspan="44">3520</td></tr>
</table>

3. Processing the Results of the First Stage of Experiments

Based on the parameters extracted from each experiment, clear results were obtained regarding which particles had lower flowability (more hang-up events) and which presented hang-ups at greater heights, depending on the filling percentage. The total mass extracted before a hang-up and the total number of hang-ups serve as the basis for calculating the hang-up frequency for each different muck. Thus, a higher amount of material extracted at the bottom opening and/or a lower number of hang-ups result in an increased hang-up frequency index as described in [14, 47] Consequently, an increase in the hang-up frequency index indicates better material flowability.

3.1 Analysing the Number of Hang-ups

The number of hang-ups was recorded across the 20 tests conducted for each particle, at the four different filling levels. Figure 5 shows the total number of hang-ups produced at the 4 filling levels for each particle, as well as the average standard deviation for each particle, considering the 20 tests across the four different filling levels.

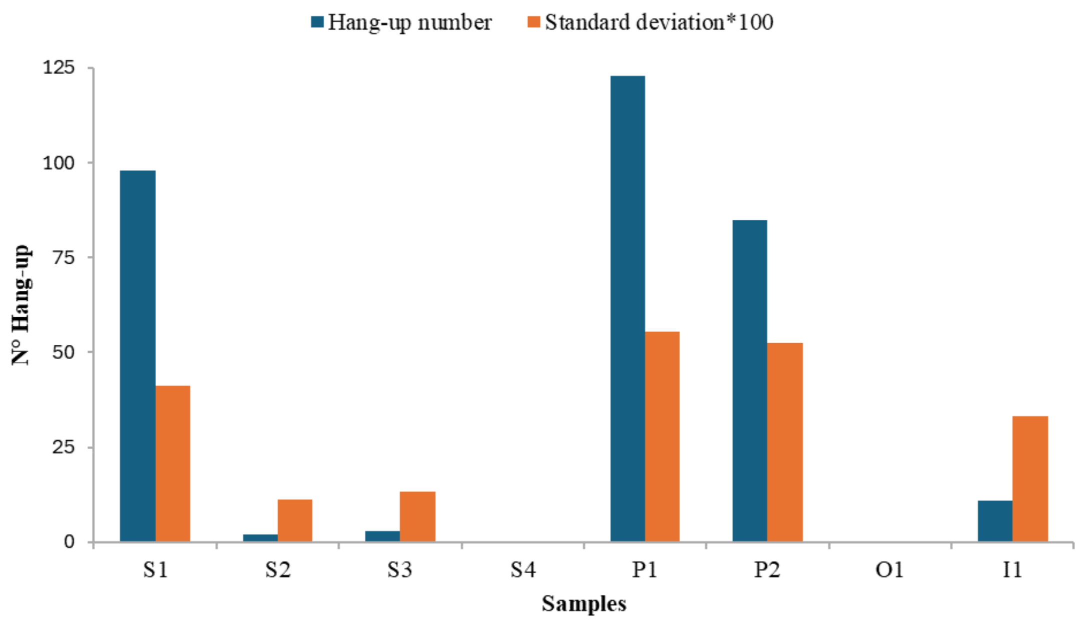

Figure 5: Total number of Hang-up for all fills percentage

The particles that did not experience any interferences in the 20 tests at each filling level were S4 (small spherical particles, d_{80} = 4.11 mm) and O1 (small irregular particles, d_{80} = 3.03 mm). In addition, referring to Table 2, the D/d ratio for muck type S4 is 7.54, and for type O1, it is 10.23. Interestingly, these findings align with [36, 25], who noted that a D/d ratio above 6 and 10, respectively, could help ensure consistent ore flow in ore passes.

In contrast, the particles that experienced more interferences were P1 (large triangular prism particles, d_{80} = 10.06 mm), S1 (large spherical particles, d_{80} = 9.99 mm), and P2 (medium triangular prism particles, d_{80} = 6.61 mm). Similarly, the D/d ratios for particles P1, S1, and P2 are 3.08, 3.1, and 4.69, respectively. Although these values all satisfy several existing criteria such as [50, 1], frequent hang-ups observed in the flow of these muck types.

Particles S4 and O1 had the smallest diameter, but with different shapes. On the other hand, P1 and S1 were the largest particles (over 9 mm), with different shapes. Taking a closer look at these results, it appears that when the pass diameter exceeds 7.0 and approaches 10 times the largest block size or d_{80}, the risk of hang-ups decreases, and particle shape becomes a secondary factor. However, when the pass size is below this range, specifically around 3.0 to 4.0 times the d_{80}, particle shape becomes a critical factor in the development of hang-ups. Particles with pyramid shapes, in particular, can cause interlocking hang-ups by wedging.

Figure 6 also shows the probability of hang-up occurrence, per particle shape and differentiated by filling percentage. It also represents the probability, in percentage terms, of experiencing at least 1, 2, or 3 hang-ups in a single extraction, with distinctions made by the filling percentages (100%, 75%, 50%, and 25%).

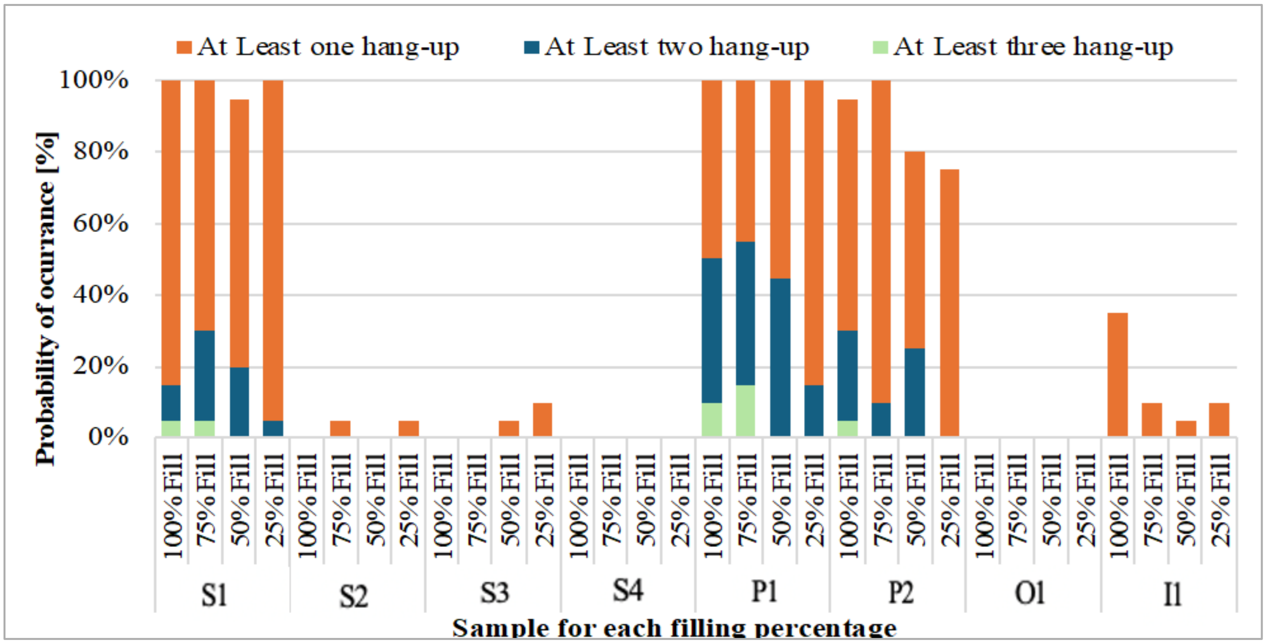

Figure 6: Probability of hang-up occurrence, for each fill percentage

In general, the highest probabilities occur when there is at least one hang-up (orange bar), specifically for samples S1, P1, and P2 (Large spherical particles, and large and medium triangular prism shape particles), with a small percentage for I1 (medium irregular particles, d_{80} =5.16 mm). Additionally, sample P1 will always produce at least one hang-up during extraction, regardless of the filling percentage (almost similar in S1). There is a lower probability of experiencing 3 hang-ups (green bars) during the same flow test, with samples S1, P1, and P2 being the only ones capable of causing 3 hang-ups in one withdrawal of the pass. For particles larger than 9 mm (S1 and P1), a filling level of at least 75% is required for there to be a probability of 3 hang-ups, and the highest probabilities of experiencing 2 hang-ups occur at a 75% filling level. This indicates that higher filling levels do not always present the highest probabilities of hang-ups, as particles S2 and S3 (medium sphere particles, d_{80} = 7.65 and 6.30 mm, respectively) show higher probabilities at lower filling levels.

Further investigation into these non-linearities is essential and could greatly benefit ore pass design. For instance, it appears that keeping ore passes full of ore materials might enhance safety without necessarily increasing the rate of hang-ups. However, the reasons behind these non-linearities are not yet clear and need further investigations. They might be related to the vertical gravitational loads acting on the particles in the pass, which push and keep them moving when the gates are opened. This idea could be controversial, as the risk of compaction may also rise when ore passes are fully filled. On the other hand, maintaining ore passes filled significantly reduces the risk of impact-induced damage and lowers the dynamic loads on the gates.

3.2 Investigating the Height of Hang-ups

The heights at which hang-ups occurred were also measured, for all the experiments, from the base of the cylinder (0 cm) for each particle type and for all the four filling levels. Figure 7 displays the recorded mean heights where hang-ups formed, depending on the filling percentage for each particle. At 100% filling, the maximum height that can be recorded is 78 cm; at 75% filling, the maximum height is 58.5 cm; at 50% filling, the maximum height could be 39 cm; and finally at 25% filling, the maximum recorded height of hang-ups can reach 19.5 cm. Particles without hang-ups in tests were not included in Figure 7 to avoid confusion with those that recorded hang-ups close to 0 cm height.

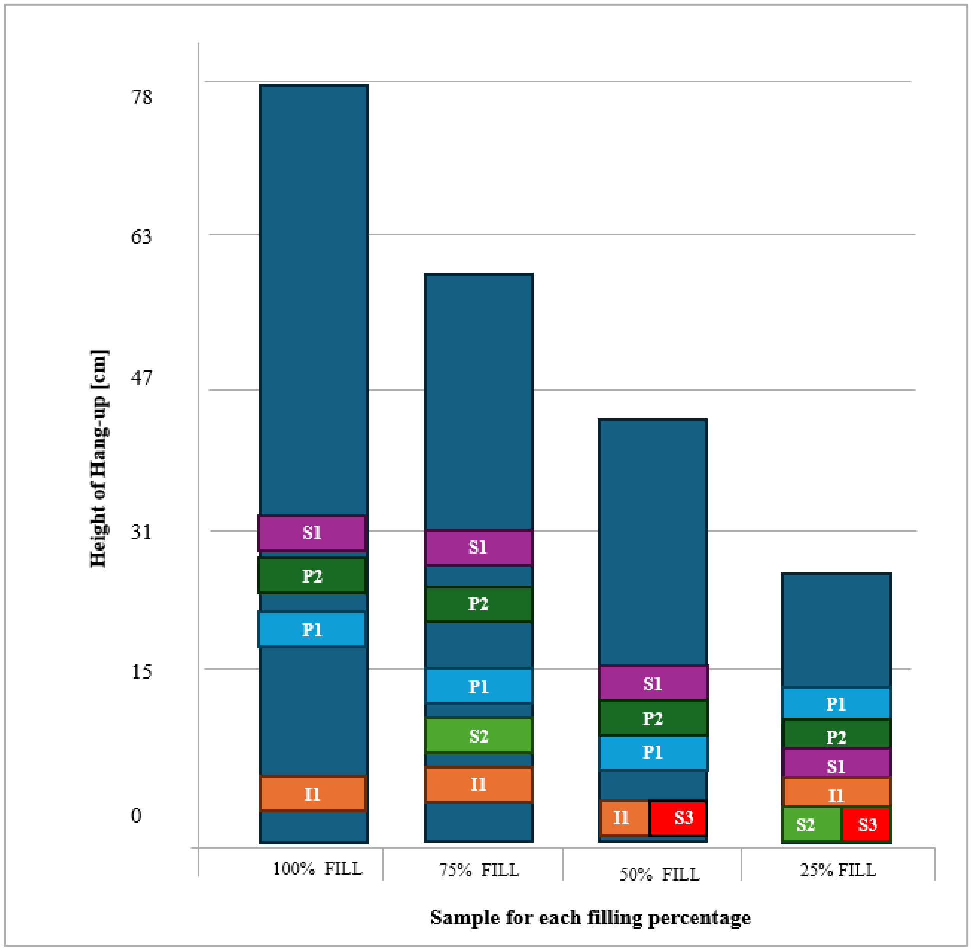

Figure 7: Height of Hang-up for each fill percentage

In Figure 7, particle S1 (large spheres) forms hang-ups at higher heights. Particle P1 is the third in terms of height of hang-ups despite to be larger than P2 (d_{80} (P1) = 10.06 mm and d_{80} (P2) = 6.61 mm). S1 and P2 particle types follow a similar behaviour, but this changes when the filling level is at 25%, with their positions reversing. Particle P2 maintains a consistent pattern across all filling levels, being the second to present hang-ups at higher heights. Particles such as I1, S3, and S2 are potentially less problematic because if they form a blockage, it occurs near the bottom of the ore pass, making it more accessible for removal. Consequently, hang-ups tend to be towards the lower end of the pass. No significant variations in hang-up height were observed with these particle types across different filling levels.

Overall, the data presented in Figure 7 suggest that when particle sizes are large (like S1) or wedge-shaped (like P1 and P2), hang-ups are more likely to occur higher up in the ore pass, which can make access for clearing them more challenging. However, if the diameter of the ore pass is seven to ten times larger than the particle sizes—regardless of shape—the likelihood of hang-ups is significantly reduced, with blockages mainly occurring closer to the gate. On the other hand, when the ore pass is only partially filled (e.g., 25% full), the muck load on an arch formed by small particles may not be sufficient to break it and maintain flow. In other words, if rock fragments are much smaller than the ore pass diameter, it is advisable to keep the pass full or nearly full to reduce the risk of interlocking hang-ups, as the higher gravitational load can help break any arch formation. This behaviour aligns with the principles of the voussoir arch theory [10, 58], which was historically applied in the design of ancient Persian and Roman architecture. It should be noted, however, that this does not account for the probability of cohesive hang-up development, which will be addressed in a forthcoming experimental paper by the authors.

3.3 Computing the Hang-up Frequency Index

Figure 8 shows the total hang-up frequency for the eight particles at their respective filling levels, considering the 20 tests per particle. As we previously stated, the hang-up frequency is defined as the amount of material that can be drawn before an interruption, such as a blockage, occurs (in grams). The filling levels are represented as follows: blue for 25% filling, orange for 50%, green for 75%, and light blue for 100% filling. A reference value of 18,000 was assigned to particles that did not record any hang-up in the 20 tests.

As can be seen in Figure 8, a similar trend is observed for the 25% and 50% filling levels, while for the 75% and 100% filling levels, particles S2 and S3 show some variations in frequency at different proportions. As the filling level increases by 25%, the hang-up frequency rises by approximately 35% for particles S2, S3, S4, O1, and I1. On the other hand, the filling level does not significantly influence the particles with lower hang-up frequencies (less than 50), such as S1, P1, and P2.

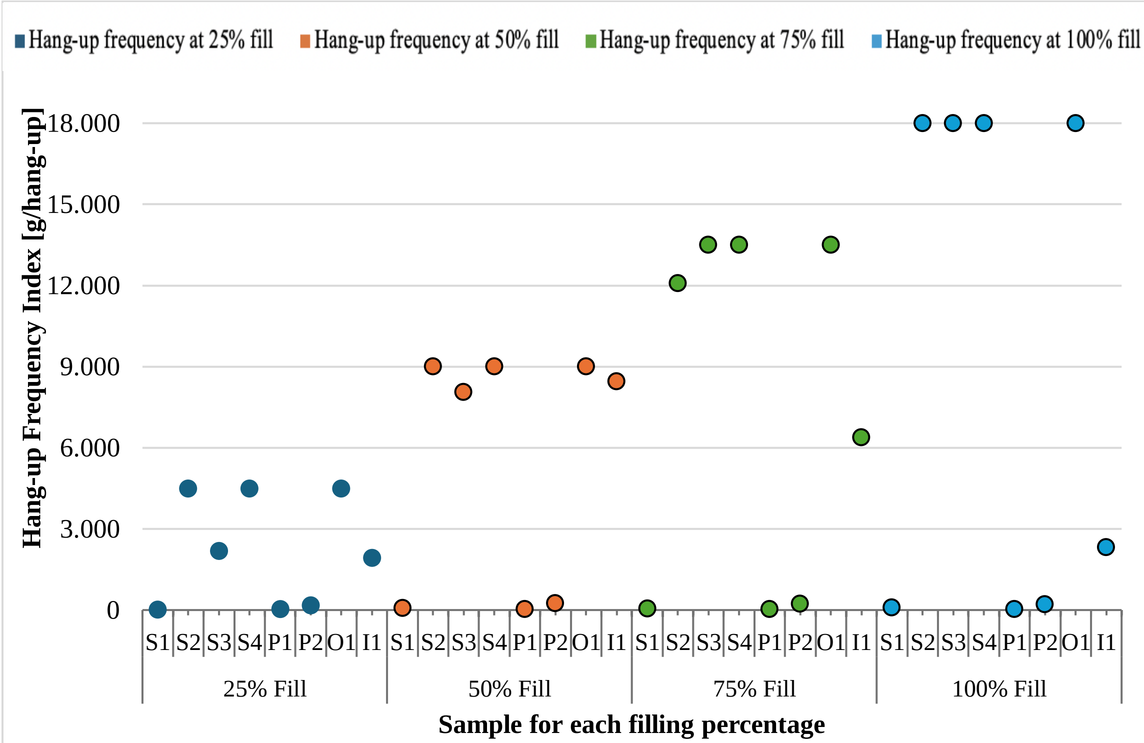

Figure 8: Hang-up frequency index, HFI, for each fill percentage

In addition, the analysis indicated that as the filling percentage increases, the difference in hang-up frequency between muck type I1 and other muck types like O1 becomes more pronounced. This suggests that muck type I1 is much less sensitive to the filling percentage compared to other types such as O1, S2, S3, and S4.

The data presented in Figure 8 suggests that increasing the filling percentage for particles that are relatively small compared to the ore pass diameter tends to improve the hang-up frequency index, resulting in better and more consistent flow. [47] a demonstrated that the hang-up frequency index (HFI) is a complex function influenced by various factors, including vertical loads, fine particle content, and moisture levels. Notably, the relationship between HFI and vertical load is highly non-linear, which accounts for the observed non-linearities in the hang-up frequency index as the filling percentage increases.

4. Processing the Results of the Second Stage of Experiments

In this second stage of experimentation, the same parameters were analysed as in the first stage, but instead of using the original eight particles, forty-four different combinations of these particles were created by blending (see Figure 3). Of these, twenty combinations (D1-D20) were made with particles of different shapes and sizes in equal proportions, twenty-one combinations (SS1-SS21) were made with spherical particles of varying sizes, and three combinations (PP1-PP3) were also made with triangular prism particles of different sizes.

4.1 Analysing the Number of Hang-ups

The number of hang-ups was recorded in the twenty tests conducted for each of the 44 particle combinations, across the four different filling levels. The composition of the different muck types has been previously discussed (see Figure 4) and is also shown in Table 6 in the Appendix. Figure 9 displays the sum of all hang-ups produced at 25%, 50%, 75%, and 100% filling levels for each mixture. Additionally, it shows the average standard deviation for each combination, considering the twenty tests across the four different filling levels.

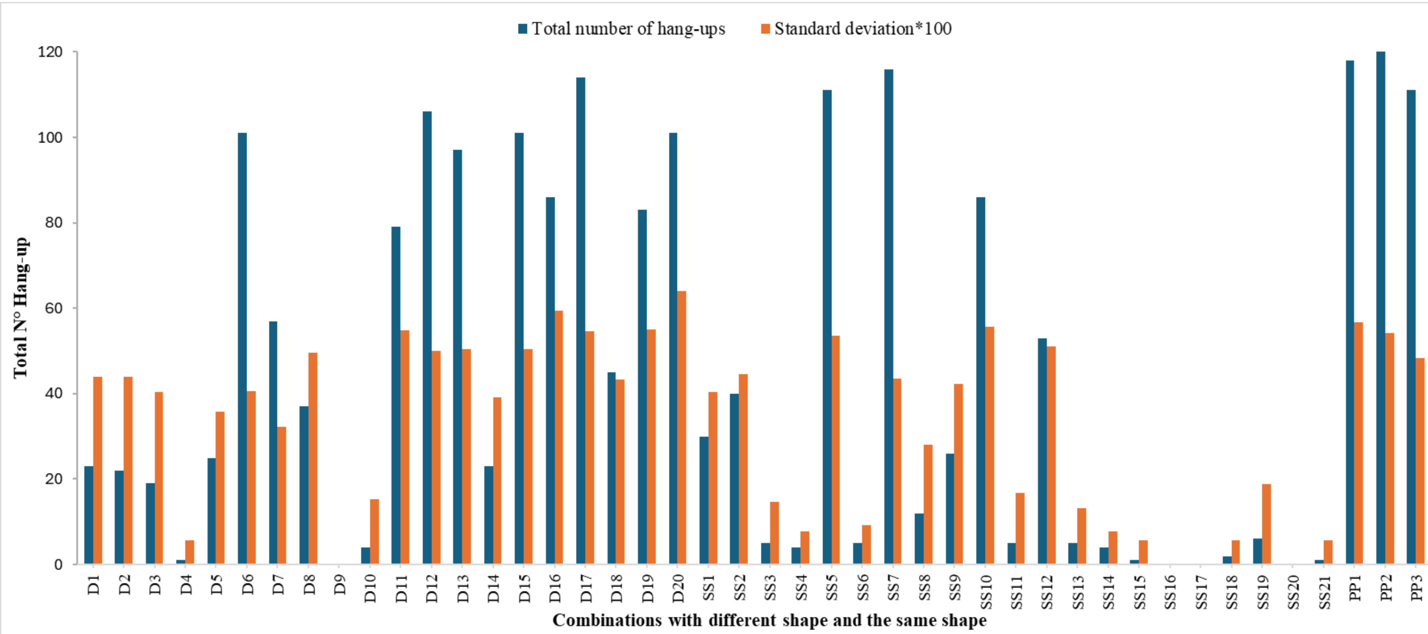

Figure 9: Total number of Hang-up for all fills percentage

The combinations that did not record any interferences in the tests were D9, SS16, SS17, and SS20 (see Figure 9 and Figure 10). D9 contains irregular medium and small particles (50% I1 and 50% O1). SS16 is composed of 80% medium spheres (S2) and 20% small spheres (S4). SS17 is composed of 20% medium spheres (S2) and 80% small spheres (S4), andSS20 featuring small spheres (20% of S3 and 80% of S4).

The combinations with the high number of interferences were D6, D12, D15, D17, D20, SS5 and SS7. Muck type D6 is also composed of equal percentages of large spherical particles (S1) and large triangular prism particles (P1). Sample D12 is formed by large triangular prism (P1) and small irregular particles (O1) in equal percentage. D15 contains equal percentages of large spherical particles (S1), large triangular prism particles (P1), small irregular particles (O1), and medium irregular particles (I1). D17 includes equal quantities of large triangular prism (P1), small irregular particles (O1), and medium irregular particles (I1). D20 contains large spherical particles (S1) and large triangular prism (P1). Additionally, SS5 consists of 80% of large spheres particles (S1) and 20% small spheres (S4). Finally, SS7 contains 80% large spherical particles (S1) and 20% medium spherical particles (S2).

Figure 10a shows the probability, in percentage, of experiencing at least 1, 2, 3, and 4 hang-ups in a single extraction, differentiated by the filling percentage (100%, 75%, 50%, and 25%). Here, the highest probabilities occur when there is at least 1 hang-up (orange bars), occurring in all combinations except for D9 and D4, where it only occurs at 100% filling, and D10, which only shows at least one hang-up at 50% and 100% filling. Furthermore, combinations D6, D12, and D17 will always produce at least one hang-up during extraction, regardless of the filling percentage.

There is a lower probability of experiencing two hang-ups (blue bars), and even less so for three hang-ups (green bars). The combinations D12, D13, D15, D17, and D20 are the only ones capable of causing three hang-ups, at

100% or 75% filling. The probability of generating four hang-ups (light blue) is the lowest and occurs only in D16 at 100% filling and D20 at 75% filling.

Particularly, combinations PP1, PP2, and PP3 have the highest number of hang-ups (see Figure 10b). PP1 consists of 20% large triangular prism (P1) and 80% medium triangular prism (P2). PP2 is made up of 80% large triangular prism (P1) and 20% medium prism (P2). PP3 has equal proportions of large triangular prism (P1) and medium triangular prism (P2).

In Figure 10b, for spherical combinations, the highest probability is for at least one hang-up (orange bar), with higher probabilities reported for combinations SS5, SS10, and SS7. The combinations made with triangular prismatic particles PP1, PP2, and PP3 always cause at least one blockage at all four filling levels. The combinations SS16, SS17, and SS21 did not produce any blockages at any filling level, although there was a slightly higher probability of occurrence in SS3 at 25%, SS4 at 75%, SS15 at 100%, and SS18 at 25% filling. The probability of experiencing two hang-ups (blue bar) is much lower and was only observed in SS5 across all filling levels, SS7 at 75% and 100% filling (which has the highest probability among all combinations), SS9 at 75% filling, SS10 at 75% and 100% filling, and SS12 at 75% filling. Notably, no spherical combinations recorded a probability of experiencing at least three hang-ups.

For combinations based on prismatic particles of different sizes, at least one hang-up (orange bars) will always occur at all filling levels. Additionally, all combinations always had a probability of experiencing at least two hang-ups (blue bars), with higher values in PP2 at 75% filling and PP3 at 100% filling, and lower values in PP1 at 75% and PP3 at 25% filling. The probability of experiencing at least three hang-ups (green bars) was much lower, recorded only in PP1 at 75% and 100% filling (with the highest value among all combinations), as well as in PP2 at 50% and 75% filling and PP3 at 100% filling.

The above findings, summarised in Figure 10, are significant, as they indicate that when particle sizes are sufficiently small (approximately 1/10 to 1/6 of the pass diameter), the influence of particle blending becomes a secondary factor in evaluating the flowability of rock fragments. However, if the particles are prism-shaped with sharp edges and vary in size, they can easily wedge together and form interlocking hang-ups, as observed in cases PP1, PP2, and PP3.

Adding small spherical particles also improves flowability to some extent. This is likely because these particles act like rollers, enhancing the movement of larger particles and those with more complex shapes.

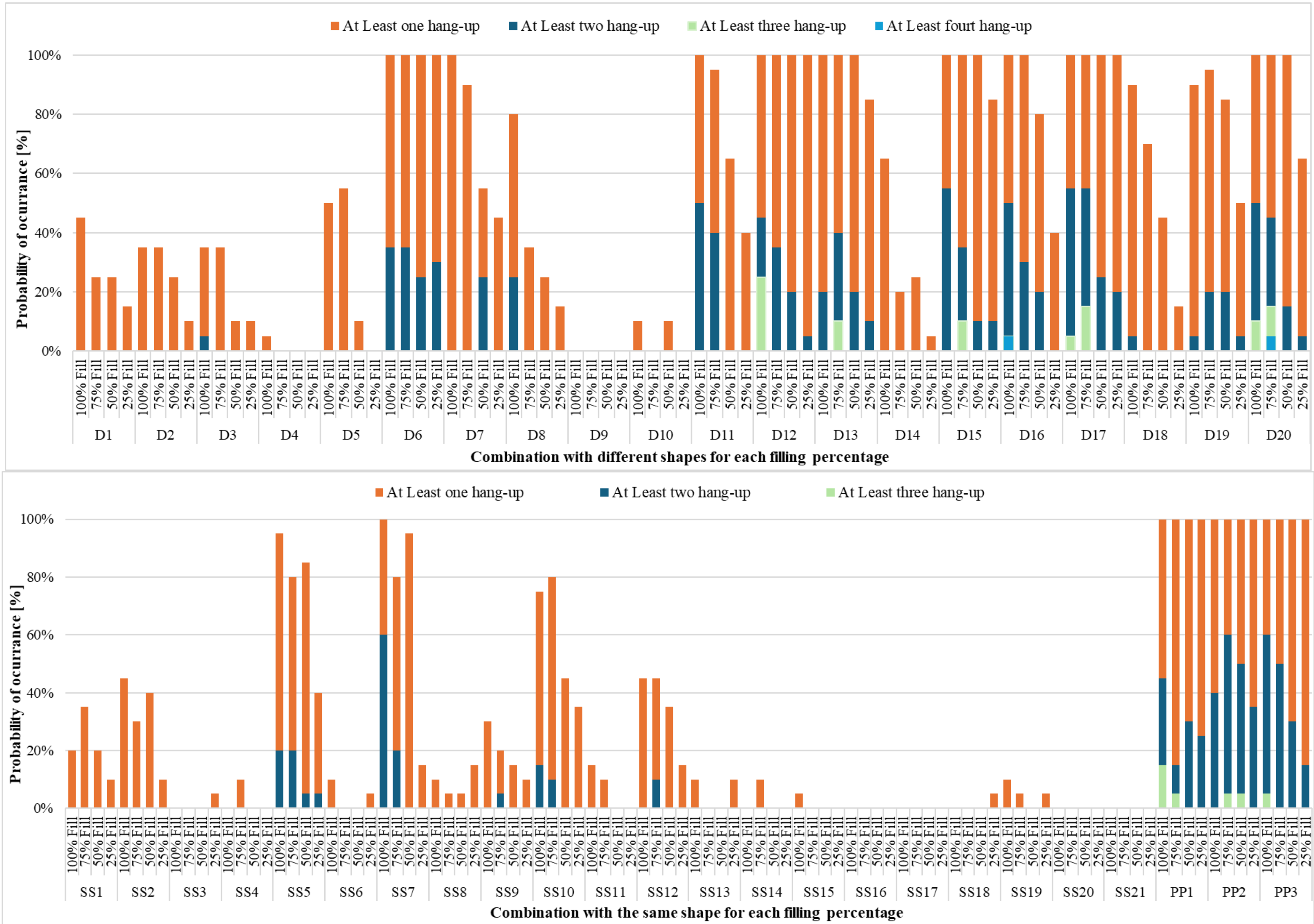

Figure 10: a) Probability of the occurrence of different number of hang-ups for combinations D1-D20 at each fill percentage, and *b) Probability of the occurrence of different number of hang-ups for combinations SS1-SS21 and PP1-PP3 at each fill percentage.*

4.2 Investigating the Height of Hang-ups

The height at which hang-ups occurred was recorded from the base of the cylinder (0 cm) for each combination at the four filling levels. Figure 11-a shows the heights at which hang-ups occurred for the combinations D1-D20 of different shapes and sizes, while Figure 11-b indicates the heights of hang-ups for spherical combinations of different sizes (SS1-SS21) and prismatic particle combinations of different sizes (PP1-PP3), based on the filling percentage for each muck type. The maximum heights recorded were 78 cm at 100% filling, 58.5 cm at 75% filling, 39 cm at 50% filling, and 19.5 cm at 25% filling. Combinations that did not produce hang-ups were excluded from the graphs to avoid confusion with those that recorded hang-ups at around 0 cm height.

As shown in Figure 11-a, the combination D8, composed of medium spheres (S2) and medium triangular prism (P2), formed hang-ups at the highest height (18.4 cm) at 100% filling. However, D20, consisting of large spheres (S1) and medium triangular prisms (P2), achieved the highest hang-up heights at 25% (3.4 cm), 50% (7.7 cm), and 75% filling (13.9 cm).

The lowest hang-ups heights were not consistently recorded for the same combinations. At 25% filling, hang-ups at 0 cm were recorded for D1, D2, D3, D8, D14, D16, and D18. Referring to Figure 4 and Table 6, muck type D1 is composed of S2, P2, O1, and I1 particles; D2, made up of S2, P2, and I1 particles. In addition, D3 contains P2, O1, and I1 particles. D8 is an integration of S2 and P2 particles. D14, consists of P2 and O1 particles. D16 has S1, P1, and O1 particles. D18, is composed of S1, O1, and I1 particles. At 50% filling, 0 cm hang-up heights were recorded for D10, composed of S1 and O1 particles, and D14, which includes P2 and O1 particles. At 75% filling, the lowest hang-ups heights were recorded for D2 and D3, both at 0 cm. D2 and D3 combinations also showing the same hang-ups height at 100% filling. These combinations share the common particle, medium triangular prism (P2).

As Figure 11-b depicts, the highest hang-up height is presented by combination SS2, composed of S1, S2, S3, and S4, at 75% filling with a height of 33.2 cm. For 100% filling, the highest hang-up heights were obtained by SS5, consisting of S1 and S4 at 26.8 cm, SS10 with particles S1 and S3, and SS11 with particles S1 and S3, both combinations reaching 26.3 cm. At 50% filling, the highest hang-up height was for SS12, containing S1 and S3 at 12.6 cm, and at 25% filling, the highest height was again recorded by SS12 at 7.7 cm. Regarding hang-ups recorded at lower heights, all cases showed hang-ups at the bottom of the pass, at 0 cm. At 100% filling, these included combinations SS6 (S1 and S4), SS13 (S2 and S3), SS19 (S3 and S4), and SS21 (S3 and S4). At 75% filling, SS8 (S1 and S2) and SS19 indicated this height, with SS8 also recording this height at 50% filling. At 25% filling, multiple combinations showed this value: SS3, SS8, SS9, SS10, SS13, SS18, and SS19.

The assessment of hang-up heights, in mucks combined of different particles, indicates that when particles of different sizes and shapes are mixed, hang-ups are more likely to occur closer to the gates at the bottom of the passes. This is likely due to the need for greater compaction load from the weight of the overlying muck to lock the particles together and form interlocking hang-ups. This effect is more pronounced when smaller spherical particles are present, as they act like rollers, facilitating the movement of larger particles—unless they are forced into the gaps between the larger particles, locking them in place. However, when larger spherical particles are introduced into the muck mix, the hang-up problem worsens, likely due to the gaps between these particles, which increase the potential for wedging when smaller sharp particles become lodged in these spaces.

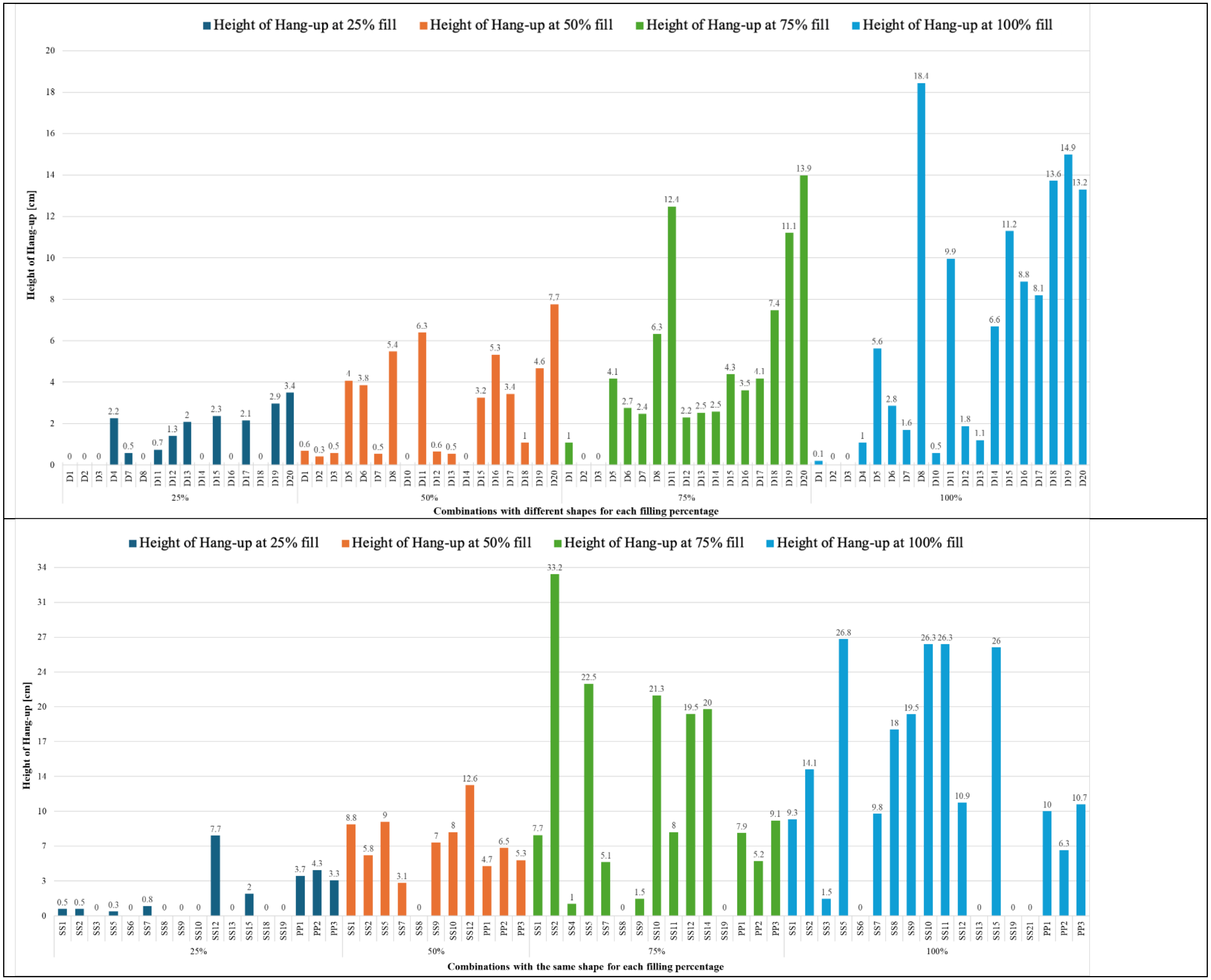

Figure 11: a) Height of Hang-up for combinations D1-D20 at each fill percentage, and b) Height of Hang-up for combinations SS1-SS21 and PP1-PP3 at each fill percentage

Figure 12 represents the average height at which hang-ups occurred for the three different combinations (D1-D20), (SS1-SS21), and (PP1-PP3). Combinations that did not register any hang-up at all four filling levels (SS16, SS17, SS20, and D9) were excluded from the graph to facilitate visualisation. Only samples that generated hang-ups at least at one filling level are included.

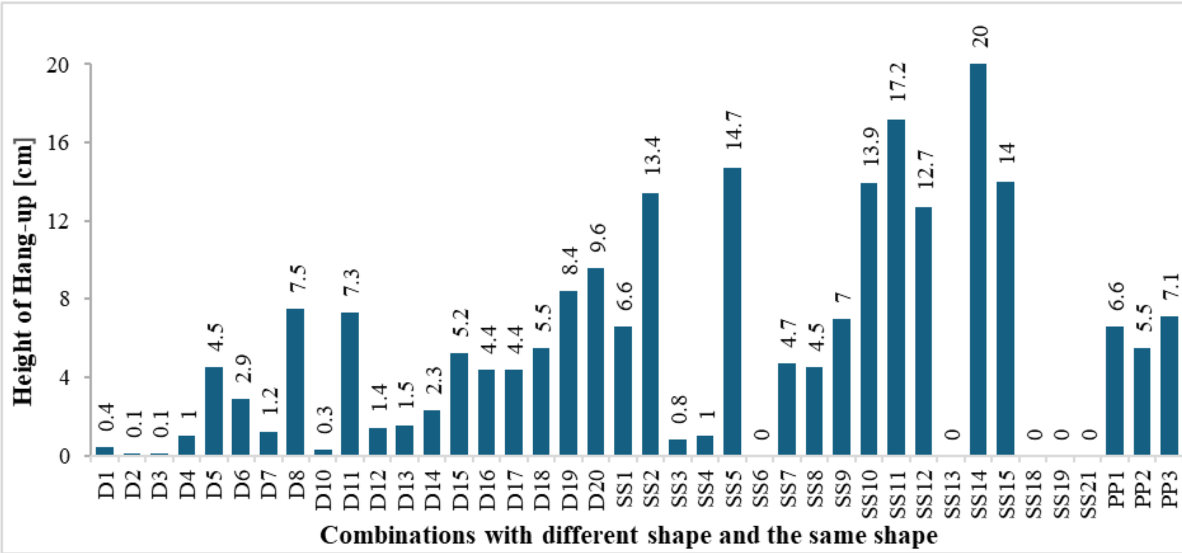

Figure 12: Height of Hang-up for all combinations at all fill percentages

In Figure 12, the combinations D1, D2, D3, D10, SS6, SS13, SS18, SS19, and SS21 generate hang-ups at lower heights (under 1 cm), while combinations SS2, SS5, SS10, SS11, SS14, and SS15 produce higher hang-ups (over 13.4 cm). Combinations made only with spherical particles (SS1-SS21) generate both the lowest and highest heights, often doubling the heights observed in other combinations. In contrast, combinations made solely with prismatic particles PP1, PP2 and PP3 register heights of up to 7.1 cm, similar to the heights recorded for circular particles SS9, SS1, and for particles D11 and D18, which vary in size and shape. The common factor among these combinations is that they all contain at least 25% of particles with a size of 6.61 mm or larger. Although some combinations of spherical particles (S1-S21) exhibit low heights, they also reach the highest heights. Therefore, combinations with relatively larger spherical particles may present more significant hang-up problems due to the greater heights they generate. This is particularly relevant for combinations SS11 and SS14, which contain 80% medium spherical particles S3 (S3, d80 = 6.3 mm).

4.3 Computing the Hang-up Frequency Index

In Figure 13, the total hang-up frequency index, *HFI*, computed for the four filling levels are presented for each of the forty-four combinations. The hang-up frequency index was calculated based on the data obtained from the mass extracted before a hang-up and the number of hang-ups produced in the 20 tests performed for each combination at each filling level. A maximum hang-up frequency index of 18,000 g/hang-up was defined when no hang-ups were recorded during the 20 tests.

Figure 13-a shows the hang-up frequency index for the 21 combinations with only spherical particles (SS1-SS21) and the 3 combinations with triangular prism particles (PP1-PP3). Blue markers represent the hang-up frequency

at a 25% filling level. Orange markers represent the hang-up frequency index computed at a 50% filling level. Green markers represent the hang-up frequency index, *HFI*, at a 75% filling level. Light blue markers represent the *HFIs* at a 100% filling level.

In Figure 13a, the lowest hang-up frequency index is related to a case where the fill level was at 100%, while the highest hang-up frequency index were recorded at a 50% fill level. The spherical combinations SS16, SS17, and SS20 maintained the highest hang-up frequency index of 18,000 g/hang-up across all levels of fill, without interruption in the 20 tests conducted per fill level. These combinations (SS16, SS17, and SS20) contained at least 20% of the smallest spherical particle (d_{80} = 4.11 mm). Conversely, the lowest hang-up frequency index (below 50 g/hang-up) was observed in the spherical particles SS5 and SS10 samples and the triangular prisms combinations PP1, PP2, and PP3, despite including at least 25% of particles larger than 9 mm (d_{80}). There are tests where hang-up frequency index increases only for spherical particle combinations at a 25% fill level, such as in SS7 sample. Additionally, some spherical particle combinations exhibit high hang-up frequency index across all fill levels except for SS21 and SS15 samples. Thus, lower fill levels might increase the hang-up frequency index, while higher fill levels might decrease the *HFI* for spherical particles. This phenomenon was not observed for PP1, PP2, and PP3 samples (triangular prism combinations).

Figure 13b also shows the hang-up frequency index for the 20 combinations with varying shapes and sizes (D1-D20). Here, blue markers represent the hang-up frequency at a 25% fill level. Orange markers represent the hang-up frequency at 50%. Green markers represent the hang-up frequency at 75%. Light blue markers represent the hang-up frequency at 100% fill level.

In Figure 13b, the hang-up frequency index of 18,000 g/hang-up represent no interruptions during the 20 tests. No hang-up events were observed when the fill level was 25% for particles D4, D5, D9, and D10, which contained at least 33.3% of small irregular particles (O1, d_{80} = 3.03 mm). Conversely, low hang-up frequency index were computed for combinations D6, D7, D11, D12, D13, D15, D16, D17, D19, and D20, regardless of the fill level. These combinations contain at least 33.3% of large triangular prism particles (P1, d_{80} = 10.06 mm) and/or large sphere particles (S1, d_{80} = 9.99 mm). There are cases where the hang-up frequency index increases when the fill level is 25%, such as in D14 and D18 combinations, but decreases significantly when the fill level is 100%. Note that muck samples D14 and D15 contain at least 33.3% of small irregular particles (O1, d_{80} = 3.03 mm). Additionally, the 20 combinations with different shapes and sizes (SS1 to SS21) exhibit lower hang-up frequency index compared to the spherical combinations but achieve higher values of *HFI* compared to the combinations made only with triangular prism particles (PP1-PP3) shown in Figure 13a.

The 24 combinations made with particles of the same shape (spherical and triangular prism) indicated that samples with a restricted range of size distribution, particularly those combinations between two particles containing a higher percentage of large size within the ore pass, had a negative impact on flowability, resulting in lower hang-up frequency index, such as PP1, PP2, PP3, and SS7. Hang-up frequency index also improved in the presence of larger particles combined with smaller particles, as seen in SS20, SS17, and SS16. The percentage of the mixture depended on the shape of the particles: for prismatic particles, the mixture percentage needed to be at least 50% to reduce hang-up frequency index, while for spherical particles, including just 20% of smaller particles was sufficient. Combinations with higher hang-up frequency index were also observed in samples with a restricted range of size distribution, provided they included at least 20% of particle S4 (4.11 mm; very small spheres) or 50% of particle S3 (6.3 mm; small spheres). In mixtures with a larger range of size distribution, the worst flow was not observed, but the hang-up frequency index remained below average. However, flow improved when the combination included at least 50% of small spherical particle S4 (4.11 mm).

Regarding samples with mixtures of different particle shapes, it was also evident that those containing a higher proportion of triangular prims particles (P1, d_{80} = 10.06 mm; and P2, d_{80} = 6.61 mm;) had a higher number of hang-ups and lower flowability. However, the addition of other sizes and shapes improved its flow, especially with much smaller particles such as O1 (d_{80} = 3.03 mm; small irregular particles) and D4 (d_{80} = 4.11 mm; small spheres particles). Additionally, the presence of larger particles led to a decrease in the D/d ratio, resulting in an increased number of blockages and negatively affecting the flow.

5. Analysis of results

The results presented show that, although particle size is a key factor in hang-up, particle shape also plays a role. In this study, particle shape is quantified through its sphericity (see Table 3). Here, Table 4 and Table 5 shows the material properties for the second stage of the experiments. Note that the values have been calculated using the weighted average of material properties of parent particles explained in stage one.

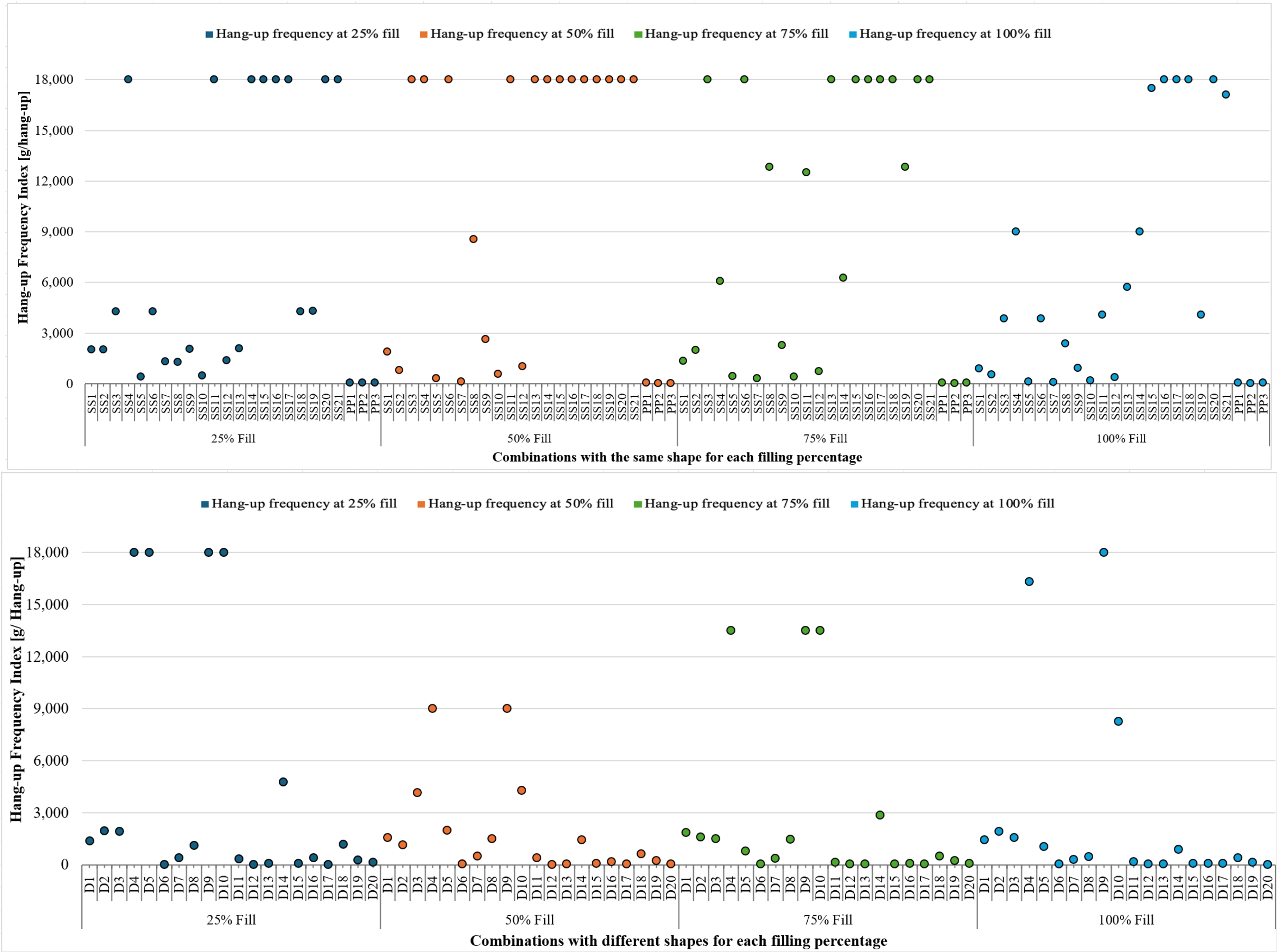

Figure 13: a) Hang-up frequency for combinations SS1-SS21 and PP1-PP3 at each fill percentage, and b) Hang-up frequency for combinations D1-D21 at each fill percentage

Table 4: Material properties, for combinations D1-D20.

Combinations Characteristics	D1	D2	D3	D4	D5	D6	D7	D8	D9	D10	D11	D12	D13	D14	D15	D16	D17	D18	D19	D20
Density [g/cm³]	10.23	8.37	9.30	8.88	10.60	6.13	10.58	7.48	12.11	7.61	8.19	19.05	7.89	8.53	14.20	8.53	14.78	10.05	8.21	6.93
Swell [%]	29.20	19.90	33.70	36.50	26.60	15.80	32.10	11.40	47.00	28.50	38.50	24.30	34.30	22.10	31.40	22.80	35.20	38.00	28.03	13.55
Uniformity coefficient [D60/D10]	2.12	2.27	1.54	1.72	1.53	1.03	1.51	1.09	1.27	3.40	2.25	3.33	2.00	2.15	3.27	3.35	1.63	3.34	1.38	1.55
Ratio D/d	5.53	5.38	6.29	5.88	4.79	3.09	5.27	4.35	7.57	4.76	4.09	4.74	4.07	6.43	4.39	4.03	5.10	5.12	4.30	3.73
Repose angle [°]	33.26	30.25	32.53	35.30	29.01	30.05	38.25	28.41	35.66	31.68	29.90	30.42	32.69	23.56	33.55	31.46	33.69	31.43	35.52	25.11
IS50 [Mpa]	11.70	10.90	10.37	14.33	11.20	13.30	8.95	9.75	13.65	16.00	16.45	10.50	10.95	8.50	13.48	13.27	11.70	15.37	12.23	11.30
Wall-combination friction [°]	20.47	16.96	25.96	18.55	20.38	13.59	28.59	15.09	25.85	12.30	17.44	22.00	27.13	23.46	19.72	15.96	24.99	18.53	20.36	15.05
Sphericity	0.87	0.88	0.79	0.85	0.86	0.91	0.80	0.90	0.77	0.90	0.91	0.80	0.79	0.82	0.84	0.87	0.77	0.87	0.88	0.94
Roughness	0.25	0.34	0.00	0.34	0.34	0.50	0.01	0.50	0.00	0.50	0.50	0.00	0.00	0.00	0.25	0.33	0.00	0.34	0.34	0.50
Simetry	0.93	0.93	0.89	0.93	0.93	0.95	0.89	0.94	0.88	0.96	0.96	0.89	0.89	0.90	0.93	0.94	0.89	0.94	0.94	0.97
Convexity	0.99	0.99	0.99	0.99	0.99	0.99	0.99	0.99	0.99	0.99	0.99	0.99	0.99	0.99	0.99	0.99	0.99	0.99	0.99	0.99

Table 5: Material properties for combinations SS1-SS20 and PP1-PP3.

Combinations Characteristics	SS1	SS2	SS3	SS4	SS5	SS6	SS7	SS8	SS9	SS10	SS11	SS12	SS13	SS14	SS15	SS16	SS17	SS18	SS19	SS20	SS21	PP1	PP2	PP3
Density [g/cm³]	7.91	7.74	8.67	8.73	6.74	7.04	5.96	5.25	6.72	6.68	7.74	6.90	7.87	7.68	8.53	7.83	8.23	8.33	8.28	9.52	9.35	9.11	7.04	7.15
Swell [%]	16.18	17.52	15.20	15.36	18.84	17.10	19.14	16.56	17.85	18.96	15.84	17.40	15.52	14.98	15.25	15.40	14.50	14.95	14.68	14.32	14.50	41.00	53.00	51.00
Uniformity coefficient [D60/D10]	1.86	1.58	1.55	1.07	2.41	2.47	1.30	1.05	1.32	1.58	1.03	1.57	1.20	1.03	1.17	1.85	1.07	1.85	1.54	1.07	1.56	1.14	1.28	1.12
Ratio D/d	4.42	3.78	5.30	5.86	3.52	4.40	3.26	3.82	3.51	3.35	4.40	3.81	4.20	4.72	4.44	4.47	6.43	5.27	5.29	6.82	5.96	4.24	3.31	3.72
Repose angle [°]	24.33	16.57	24.66	20.85	23.01	21.48	14.25	14.14	13.93	22.48	12.15	18.58	19.68	17.48	14.93	20.85	18.57	19.83	22.66	22.43	21.80	29.43	30.22	34.70
IS50 [Mpa]	19.95	24.33	21.76	24.24	20.16	22.20	18.18	16.32	17.25	18.98	19.52	19.25	16.50	18.90	17.70	17.68	23.62	20.65	20.88	24.42	22.65	13.38	13.92	13.65
Wall-combination friction [°]	3.41	3.63	3.12	2.86	3.63	3.25	3.91	3.95	3.93	3.74	3.31	3.53	3.81	3.32	3.57	3.70	2.87	3.29	3.05	2.71	2.88	23.86	25.62	24.74
Sphericity	0.97	0.98	0.97	0.97	0.97	0.97	0.98	0.98	0.98	0.98	0.98	0.98	0.98	0.98	0.98	0.97	0.97	0.97	0.97	0.97	0.97	0.84	0.82	0.82
Roughness	0.96	0.98	0.96	0.97	0.98	0.97	0.98	0.99	0.98	0.98	0.98	0.98	0.98	0.98	0.99	0.98	0.97	0.97	0.98	0.96	0.97	0.28	0.13	0.00
Simetry	0.98	0.99	0.98	0.99	0.99	0.99	0.99	0.99	0.99	0.99	0.99	0.99	0.99	0.99	0.99	0.99	0.99	0.99	0.99	0.98	0.98	0.91	0.91	0.91
Convexity	1.00	1.00	1.00	1.00	1.00	1.00	1.00	1.00	1.00	1.00	1.00	1.00	1.00	1.00	1.00	1.00	1.00	1.00	1.00	1.00	1.00	0.99	0.99	0.99

Figure 14, shows the hang-up frequency index in relation to the geometric variables: D/d ratio and particle sphericity. Figure 14a and Figure 14b demonstrate the ratio D/d and sphericity both as functions of hang-up frequency index for all particles and combinations, respectively.

In addition, Figure 15, indicates the hang-up frequency index compared to material characteristics including density and repose angle. Figure 15a and Figure 15b show density and repose angle both as functions of hang-up frequency index for all particles and combinations, respectively.

Circular markers represent spherical particles and combinations made from them (S1-S4, SS1-SS21). Triangle markers denote triangular prism particles and combinations of them (P1, P2, PP1-PP3). Diamond markers represent irregular particles (O1, I1). Square markers represent combinations made with various shapes and sizes (D1-D20).

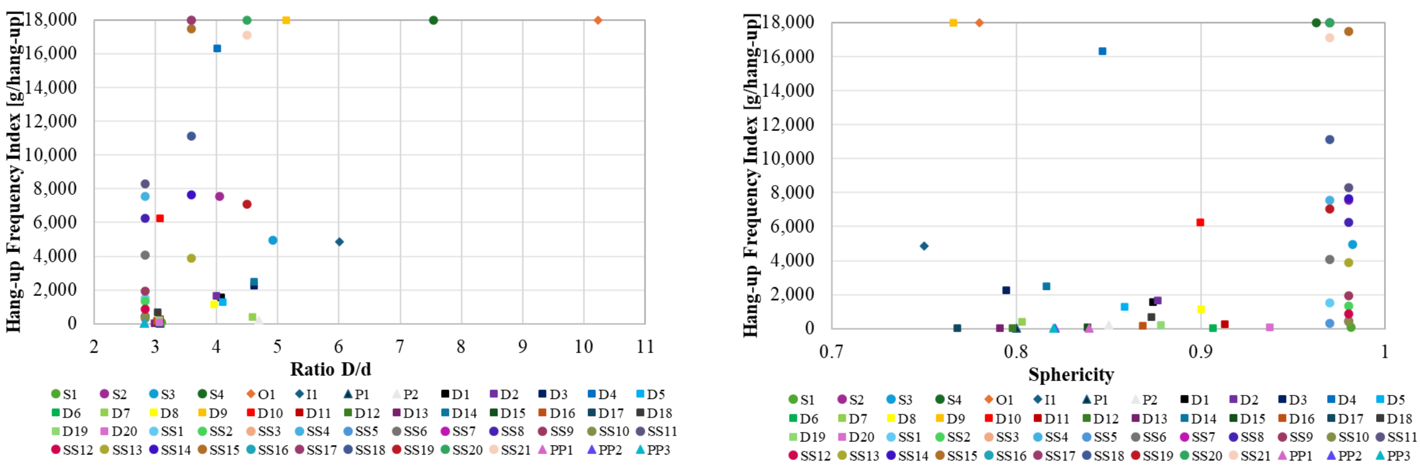

(a) (b)

Figure 14: a) Hang-up frequency index as a function of ratio D/d for all particles and combinations (D = d80), and b) Hang-up frequency index as a function of sphericity for all particles and combinations

As can be seen in Figure 14a, lower ratios of D/d reduce the hang-up frequency index, such as in samples P1 with a ratio of 3.08 and S1 with a ratio of 3.1 (P1=32.7 g/hang-up; S1=63.4 g/hang-up). In contrast, with D/d ratios over 4 the flow is considerably better or almost uninterrupted, with free flow observed in particles O1 and S4 (which have the highest ratios of 10.23 and 7.54, respectively). Moreover, the combinations D9 (composed of O1 and I1), SS17 (composed of S4 and S2), and SS20 (composed of S4 and S3) present favorable hang-up frequency index (18000 g/hang-up). The behaviour of the combinations is clearly influenced by particle diameters, where particles with very low D/d ratio show a high tendency to interlock, such as D12 (composed of P1 and O1; 29.8 g/hang-up), D6 (composed of S1 and P1; 28.3 g/hang-up), and PP2 (composed of P1 and P2; 26.74 g/hang-up). Conversely, combinations with higher D/d ratio particles tend to have a higher hang-up frequency index showing a better flowability.

Figure 14b also shows the effect of sphericity on hang-up frequency index. The results show a slight trend towards improved flowability with increased sphericity of the particles. Samples with the highest hang-up frequency index, reaching up to 18000 g/hang-up, include S4 (sphericity 0.96), SS20 (sphericity 0.97), and SS17 (sphericity 0.97). However, similar values of hang-up frequency index were also obtained for samples with minor sphericity, such as O1 (sphericity 0.78) and D9 (sphericity 0.77). On the other hand, samples with lower hang-up frequencies index include some samples with high sphericity such as D6 (sphericity 0.91; 28.3 g/hang-up) and S1 (sphericity

0.98; 63.4 g/hang-up). This indicates that as the fragment dimensions increase (i.e., at lower D/d ratios), the influence of sphericity becomes a secondary or lesser effect.

The influence of sphericity becomes noticeable when considering it together with the ratio (D/d). For example, the medium triangular prism particles P2, which have a high ratio (4.69) and low sphericity (0.85), showed significantly lower hang-up frequency index compared to the medium spherical sample S2, which has a lower D/d ratio (4.05) and high sphericity (0.98) (P2=208.2 g/hang-up; S2=7533.7 g/hang-up). Similarly, medium irregular particles (I1) with low sphericity (0.78) and high ratio (6.01) exhibited fewer hang-ups than medium spherical particles (S3) which has high sphericity (0.98) and a D/d ratio of 4.92 (I1=4857.3 g/hang-up; S3=4957.8). This shows that greater friction and interlocking among angular and irregular particles decrease flow through the model, whereas spherical particles flow more efficiently.

It is also notable that the relationship between particle size and flowability is not the only relevant variable; other factors can also have a significant impact on the flowability. Regarding other material characteristics investigated in this study, Figure 15a shows the relationship between density and the hang-up frequency index, while Figure 15b shows the repose angle effect on the hang-up frequency index. It was observed that density (see Figure 15a) did not provide clear trends regarding flow behavior in the evaluated cases.

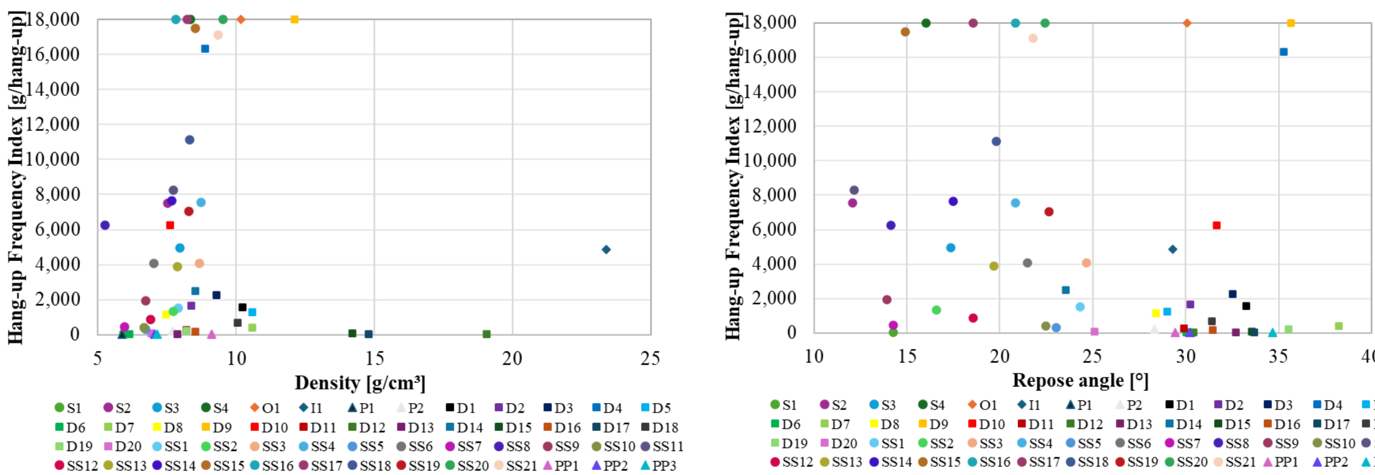

(a) (b)

Figure 15: a) Hang-up frequency index as a function of density for all particles and combinations, and b) Hang-up frequency index as a function of repose angle for all particles and combinations

The repose angle (Figure 15b) was identified as a factor the have an influence on granular material flowability. Samples with lower repose angle, such as spherical particles, showed better hang-up frequency index (18000 g/hang-up), such as S4 (16.0º), SS16 (20.9º), SS17 (18.6º). This can be attributed to the lower internal friction or interlocking and major movement of spherical particles. However, S2 (12.1º), and S3(17.4º) samples were noteworthy regarding hang-up frequency index, with S2 presenting a value of 7533.7 g/hang-up and S3 with a *HFI* of 4957.8 g/hang-up, despite their ratios suggesting that S3 should have had a higher hang-up frequency index. This suggests that in these cases, the repose angle may have been the determining factor, aligning with the fundamental theory proposed by [12].

In contrast, triangular prims samples P1 (30.26º; 32.7 g/hang-up) and P2 (28.30º; 208.2 g/hang-up), along with combinations containing these particles, such as D6 (30.05º; 28.3 g/hang-up), D12 (30.42º; 29.8 g/hang up), D13 (32.69º; 40.5 g/hang-up), PP2 (30.2º; 26.7 g/hang-up), and PP3 (34.7º; 40.4 g/hang-up), exhibited greater hang-up problems due to higher friction and irregular particle shapes, which result in lower hang-up frequency index. Notably, I1 (29.30º; 48.57 g/hang-up) and O1 (30.10º; 18000 g/hang-up) have high repose angles, and their hang-up frequency index is high compared to S1, which has a low repose angle and lower hang-up frequency (14.3º; 63.4 g/hang-up), this aligns with the previous observation that the flow behaviour of particles with very large dimensions relative to the pass diameter are less influenced by other characteristics. In other words, when assessing the flowability of large particles with a low D/d ratio, the repose angle becomes a secondary factor or of lesser importance.

6. Discussion

The literature suggests that a higher ratio of ore pass diameter to particle diameter can reduce hang-ups events, thereby facilitating material handling. However, in this study, which involved a wide variety of particles and combinations, the influence of additional variables was quantified, providing valuable data. Higher ratios did not always translate to fewer hang-ups, particularly in combinations with different particle shapes and sizes. In contrast, for combinations with particles of the same shape, spherical particles showed a trend where a lower D/d ratio resulted in fewer hang-ups, although this behaviour was only observed in some combinations. This is especially relevant in mining where we can find various particle shapes and sizes. Although the size of rock fragments in mining has been extensively studied, with numerous methods available for predicting particle size distribution in stope blasting [48], the shape of rock fragments has received much less attention. One of the most fundamental studies on the shape of rock fragments in mining was conducted by the Soviet scholar Professor Leser Isacovich Baron. To further understand the role of fragment shapes, it is useful to briefly review the work of this scholar. According to [2], a rock fragment is described by three dimensions ($a \geq b \geq c$) (see Figure 16). These three values of a, b, and c are known as the length, width, and thickness of the rock fragment, respectively.

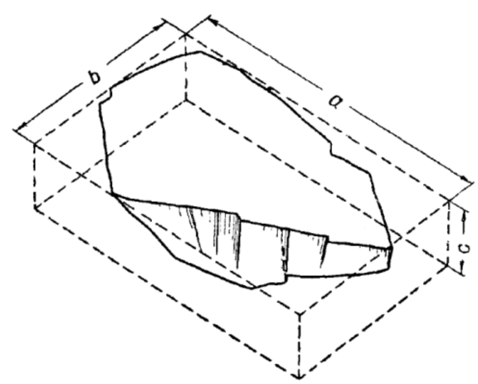

Figure 16: Schematic view of a rock fragment shape (Adopted from [2])

The particle-size distribution indicates how these fragments are spread out based on their sizes. Shape characteristics are determined by the ratios of (a/b) and (c/b). These ratios are averaged across the entire rock and subsets of fragments where the ratios of (a/b) or (c/b) exceed a specific value (see Figure 17).

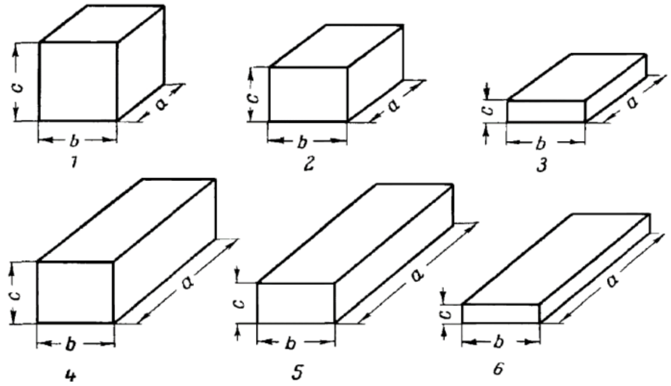

Figure 17: Different hypothetical forms of rock fragments. 1- Cubical shape [a = (1.0 to 1.3)×b and c =(0.7 to 1.0)×b]; 2 - tabular shape [a = (1.0 to 1.3)×b and c =(0.3 to 0.7)×b]; 3 - planar shape [a = (1.0 to 1.3)×b and c <0.3×b]; 4- columnar shape [a>1.3×b and c =(0.7 to 1.0)×b]; 5 - elongated-tabular shape [a>1.3×b and c= (0.3 to 0.7)×b]; and 6 - elongated planar shape [a>1.3×b and c<0.3×b] (Adopted from [2])

[2] applied this methodology to examine the morphology of rock fragments across multiple mining sites which we extracted for further analysis to investigate the complexity of the fragment shapes in real mining cases. For example, the rock particle shape data depicted in Figure 18 are related to the Sokolny gold mine in Kazakhstan. As can be seen, most of these fragments exhibit columnar, followed by cubical, elongated tabular, and tabular shapes. However, occurrences of elongated planar or planar shapes are notably scarce.

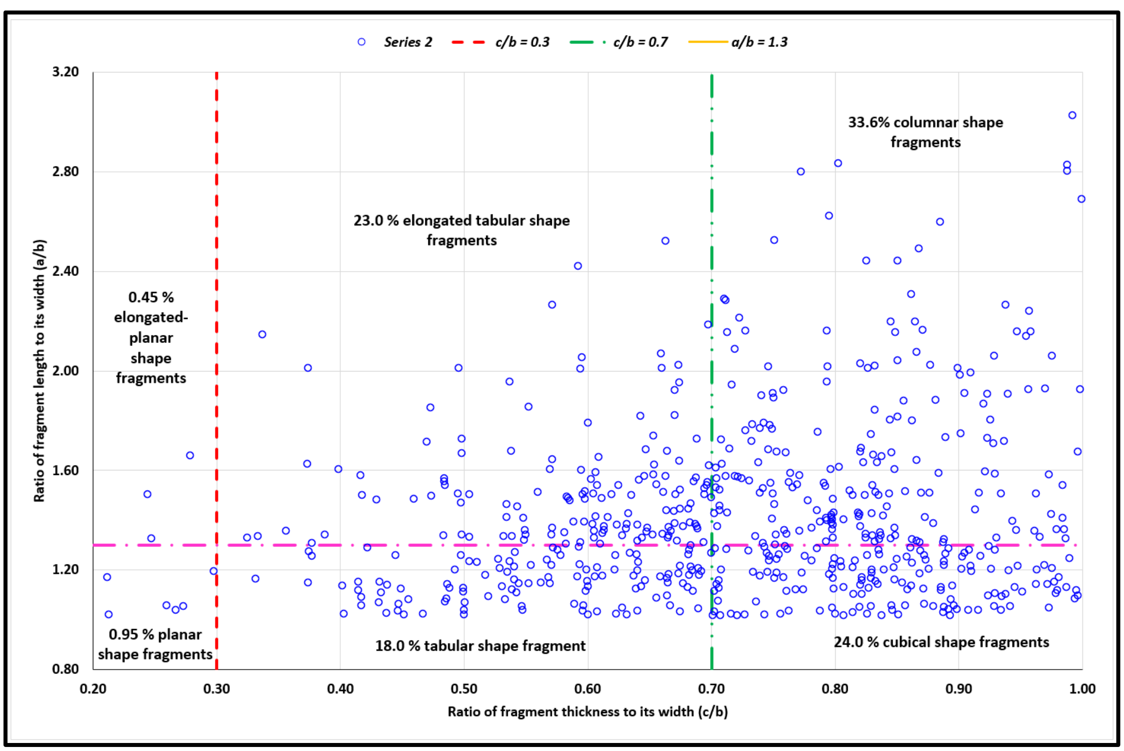

Figure 18: The distribution of characteristic parameters describing the shapes of rock fragments.1 - elongated planar shape particles: 0.45%; 2 - elongated – tabular shape particles: 23.0%; 3 - columnar shape particles: 33.6%; 4 - planar shape particles: 0.95%; 5 -

tabular shape particles: 18.0%; 6 – cubical shape particles: 24.0% (Data related to block No. 3 of the second Innokenty-evskaya lens at the Sokolny mine in Kazakhstan) (Data collected from [2])

Figure 19 also show the histogram of length and thickness of rock particles over their width. As can be seen the histogram, the length over width, (*a/b*) is positively skewed meaning that significant number of the particles has a (*a/b*) ratio of smaller than 1.3 while the (*c/b*) ratio distribution is slightly negatively skewed with the dominant value around 0.6 to 0.9 which indicates cubical shape. However, the dominant type of particles based on the definition shown in Figure 17 is columnar. This is because columnar shape class is wide in such a way that it contains wider particles lengths showing the complexity of quantifying the real shapes of rock fragments due to the no upper limit for the (*a/b*) ratio.

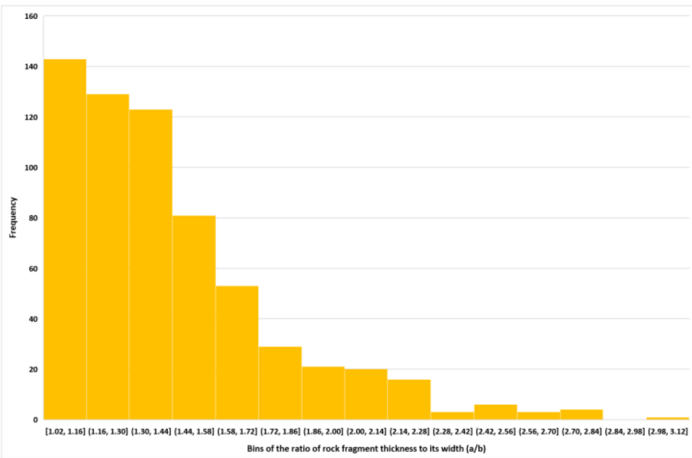

(A)

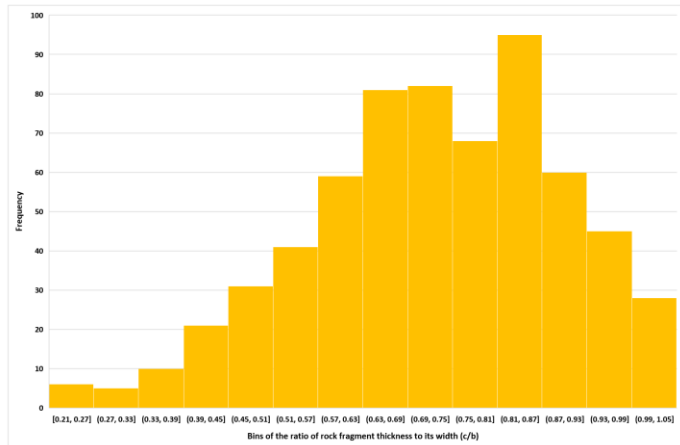

(B)

Figure 19: Histogram of the ratios of fragment A - length and B - thickness over width based on data shown in Figure 18

Investigating the data captured in the studies by [2], indicated that, in reality, muck in mines contains rock fragments of varying sizes and shapes. This highlights the need for greater attention to these details in order to enhance the efficiency of ore transport in ore passes within deep underground mines.

Angular particles tested, in our study, also exhibited a high tendency to block due to greater friction with the ore pass walls (despite its low friction wall) and among themselves because of their shape. However, controlling particle shape and ensuring some degree of sphericity in an operational environment is extremely challenging as the shape of rock fragment is mainly controlled by geology and to some extent by the blast design [17]. The natural variability in rock size and shape makes it challenging to achieve an ideal form for continuous flow. Therefore, it is advisable to incorporate some flexibility in ore pass designs, especially if angular particle geometries are anticipated. This can potentially be achieved by designing ore passes with a higher dimension, such as a D/d ratio of 6 to 10, consistent with the values proposed by [38, 27]. However, it should be noted that increasing the dimension of the ore pass can substantially raise stability issues and significantly increase the cost of raise boring and stabilization [44]. For future experimental trials, it is recommended to include additional variables such as different ore pass geometries (square or rectangular shapes) and assess their viability with longer lengths. It is also important to consider fragmentation during extraction, especially in long ore passes due to the observed trend of increasing the probability of blockage occurrence as particles traverse greater distances, although not to the same extent in all cases. It would also be beneficial to investigate how the inclination of ore passes affects the flowability of different rock fragments. Additionally, using various materials for the tube to better simulate real ore pass wall conditions, thereby increasing friction between the wall and particles, is suggested. This approach is expected to result in more hang-up events.

Controlling the homogeneity of the particle mixture entering the ore pass is also recommended. Observations show that when particles are sorted by size and shape, larger particles often fall first into the cylinder, leading to interlocking and obstructing flow. Conversely, a more uniform particle distribution, incorporating both large and small sizes, can enhance flow efficiency.

7. Conclusion

The results obtained through the physical models in this study have been crucial in understanding the impact of different particle combinations, differentiated by size and shape, on the frequency of hang-ups and the flowability of mucks. The concept of hang-up frequency index was adopted and applied for investigating the flowability of different muck types. By comparing the results from the 44 combinations with the 8 original particle types, it was observed that adding particles with higher hang-up frequency index to a particle with a lower hang-up frequency index it is possible to reduce the generation of interferences. However, the impact varies and primarily depends on the shape, size, and proportion of the particles involved. In practical mining engineering, achieving this can be partially accomplished by adjusting the ring blast design. Enhancing the uniformity of explosive distribution and increasing the powder factor to a specific level can help achieve more uniform fragmentation and reduce the size of larger particles. Additionally, employing grizzlies and implementing secondary breakage at the tipping point can also be beneficial. It was also observed that the number of hang-ups can be significantly reduced by combining certain types of particles, even when some of these particles individually caused a high frequency of hang-ups. The combinations that generated the most significant negative impacts, decreasing the hang-ups frequency index, involved medium prism particles (P2; d_{80} = 6.61 mm) with 80% larger triangular prism particles (P1; d_{80} = 10.06 mm), which reduced the hang-ups frequency index by 87.65%. For the smaller spherical particles (S4; d_{80} = 4.11 mm), the presence of 80% larger spherical particles (S1; d_{80} = 9.99 mm) decreased the hang-up frequency index by 99.45%. For irregular particles (O1; d_{80} = 3.03 mm), 80% of large triangular prism particles (P1; d_{80} =10.06 mm) reduced the hang-up frequency index by 99.9%. Finally, for medium irregular particles (I1; d_{80} = 5.16 mm), 80% of larger triangular prism particles (P1; d_{80} = 10.06 mm) decreased the hang-up frequency index by 99.1%.

On the other hand, the combinations that had the most positive impact, increasing the hang-ups frequency index, were 80% of smaller spherical particles (S3; 6.30 mm) with 20% of larger spherical particles (S1; 9.99 mm), which increased the hang-up frequency index by 14317%. For medium prismatic particles (P2; 6.61 mm), adding particles of two different types (I1; 5.16 mm and O1; 3.03 mm) in the same proportion resulted in a 770% increase in the *HFI*. For particles with no distinct shape pattern (I1; 5.16 mm), 80% of irregular particles (O1; 3.03 mm) led to a 1169.5% increase in the hang-up frequency index. In summary, the incorporation of large spherical and triangular prismatic particles (S1; d80 = 9.99 mm; P1; d80 = 10.06 mm) had the most significant impact on increasing the risk of hang-ups. Conversely, adding some type of smaller particles to those particles with low hang-ups frequencies index can significantly reduce the occurrence of hang-ups, thereby decreasing interference.

The analysis of hang-up frequency index, computed for different muck types, revealed that the ration of pass diameter to the particle size (shown as D/d ratio), sphericity, and repose angles significantly impact flowability. Lower D/d ratios generally decrease hang-up frequency index, while ratios above 4 results in nearly uninterrupted flow and high ratios of D/d correlate with improved flow. Sphericity has a nuanced effect; while higher sphericity generally enhances flowability, particles with low sphericity but high D/d ratios can still exhibit reduced hang-ups.

Additionally, it was observed that combining sizes with a 23.47% reduction in particle sphericity could lead to up to a 98.48% decrease in hang-up frequency index. In contrast, dealing with a single particle size and shape showed that an 18.37% decrease in sphericity resulted in a 46.92% reduction in hang-up frequency index. This indicates that the impact of reducing sphericity is more pronounced when particles are combined with other sizes. The relationship between particle size and flowability is complex, with sphericity and repose angle also playing critical roles. Particles with lower repose angles, often spherical, exhibit better flowability due to reduced internal friction and interlocking. Conversely, particles with higher repose angles and irregular shapes face greater hang-up challenges. Overall, optimal flowability is a function of a combination of high ratio, suitable sphericity, and favorable repose angle, with specific particle characteristics influencing the extent of hang-ups.

An appropriate configuration could minimise material handling interferences in ore passes, potentially reducing the need for alternative diesel equipment. This would contribute to decarbonisation and enhanced system performance in underground mining. The findings of this study provide valuable insights into the characterisation of the flowability behaviour of granular rock-like materials. While the ratio between particle size and ore pass diameter significantly influences hang-ups, other factors such as particle shape and particle size distribution can also substantially impact the occurrence of hang-ups. Therefore, these parameters should be carefully considered in the design of ore passes, and specifically long ore passes.

Acknowledgments

The authors express their sincere gratitude to CSIRO for the opportunity to collaborate with them and for their invaluable financial support throughout this research project. We are also grateful to the University of Concepción and the Department of Metallurgical Engineering for their support and assistance. Additionally, we wish to express our gratitude to Dr. Constanza Paredes and Dr. Ewan Sellers for their trust, guidance, and for making this work possible.

8. References

[1] Aytaman, V. 1960. Causes of hanging in ore chutes and its solution. Canadian Mining Journal, **81**, 77-81.

[2] Baron, L.I. 1960. Lumpiness and methods of its measurement. Publishing House of the USSR Academy of Sciences, Moscow.

[3] Beus, M.J., Pariseau, W.G., Stewart, B.M. & Iverson, S.R. 2001. Design of ore passes. *In*: Hustrulid, W.A. & Bullock, R.L. (eds.) *Underground mining methods: engineering fundamentals and international case studies*. Society for Mining, Metallurgy, and Exploration, 627-634.

[4] Blight, G.E. & Haak, B.G. 1994. Tests on model underground ore passes. Bulk Solids Handling, **14**, 77-81.

[5] Bloss, M., Harvey, P., Grant, D. & Routley, C. 2011. Underground ore movement. *In*: Darling, P. (ed.) *SME Mining Engineering Handbook* Society for Mining, Metallurgy & Exploration (SME), Englewood, New Jersey, 1271-1294.

[6]Brady, J.T., Owers, N.F. & Annear, C.H. 1969. Ore breaking and handling at the CSA mine, Cobar. *Australasian Institute of Mining and Metallurgy*. AusiMM, 7-15.

[7]Brenchley, P.R. & Spies, J.D. 2006. Optimizing the life of ore passes in a deep-level gold mine. Journal of the Southern African Institute of Mining and Metallurgy, **106**, 11-16.

[8]Bunker, K.A., Campbell, A.D., O'Toole, D. & Penney, A. 2015. Guidelines for orepass design in a sublevel cave mine. *In*: Potvin, Y. (ed.) *The International Seminar on Design Methods in Underground Mining*. Australian Centre for Geomechanics, Perth, WA, Australia, np. 1-14.

[9] Butcher, R., Stacey, T.R. & Joughin, W.C. 2005. Mud rushes and methods of combating them. Journal of the Southern African Institute of Mining and Metallurgy, **105**, 817-824.

[10] Cain, W. 1893. The Stone Arch. Journal of the Elisha Mitchell Scientific Society, **10**, 32-43.

[11] Cain, W. 1905. Theory of voussoir arches. Third Edition ed. D. Van Nostrand Company.

[12] Carr, R.L. 1965. Evaluating flow properties of solids. Chemical Engineering, **72**, 163-168.

[13] Castro, R., Betancourt, F., Gómez, R., Salas, O. & Zarabia, J. 2023a. Experimental study of mudrush mechanisms under different moisture contents in block caving. International Journal of Mining, Reclamation and Environment, **37**, 243-254, doi: https://doi.org/10.1080/17480930.2023.2166761.

[14] Castro, R., Gómez, R. & Hekmat, A. 2016. Experimental quantification of hang-up for block caving applications. International Journal of Rock Mechanics and Mining Sciences, **85**, 1-9, doi: https://doi.org/10.1016/j.ijrmms.2016.02.005.

[15] Castro, R., Perez, Á. & Gomez, R. 2023b. Evaluating wet muck risk in block caving mines: A new model. International Journal of Rock Mechanics and Mining Sciences, **170**, 105485, doi: https://doi.org/10.1016/j.ijrmms.2023.105485.

[16] Castro, R.L., Fuenzalida, M.A. & Lund, F. 2014. Experimental study of gravity flow under confined conditions. International Journal of Rock Mechanics and Mining Sciences, **67**, 164-169, doi: https://doi.org/10.1016/j.ijrmms.2014.01.013.

[17] Chertkov, V.Y. 1991. Characteristics of the shape of blasted rock fragments. Journal of Mining Science, **27**, 528-532, doi: 10.1007/BF00711044.

[18] Esmaeili, K. 2010. *Stability analysis of ore pass systems at Brunswick Mine.* PhD Thesis, University of Laval.

[19] Esmaeili, K. & Hadjigeorgiou, J. 2011. Selecting ore pass-finger raise configurations in underground mines. Rock mechanics and rock engineering, **44**, 291-303.

[20] Esmaeili, K. & Hadjigeorgiou, J. 2014. Impact-induced damage on foliated ore pass walls. CIM Journal, **5**, 39-47.

[21] Gardner, L.J. & Fernandes, N.D. 2006. Ore pass rehabilitation-case studies from Impala Platinum Limited. Journal of the Southern African Institute of Mining and Metallurgy, **106**, 17-23.

[22] Gómez, R. & Castro, R. 2022. Experimental Quantification of Granular Material Fragmentation Due to Travel Distance. Mining, Metallurgy & Exploration, **39**, 615-623, doi: 10.1007/s42461-022-00545-9.

[23] Gómez, R., Castro, R.L., Casali, A., Palma, S. & Hekmat, A. 2017. A Comminution Model for Secondary Fragmentation Assessment for Block Caving. Rock mechanics and rock engineering, **50**, 3073-3084, doi: 10.1007/s00603-017-1267-2.

[24] Gómez, R., Sanhueza, V., Fustos, R. & Nelis, G. 2022. A New Approach for Hang-Up Prediction in Block Caving Mines Based on Drawbell Geometry and Vertical Stress. Mining, Metallurgy & Exploration, **39**, 2393-2400, doi: 10.1007/s42461-022-00685-y.

[25] Goodwill, D.J., Craig, D.A. & F, C. 1999. Ore pass design for reliable flow. Bulk Solids Handeling, **19**, 13-21.

[26] Hadjigeorgiou, J., Esmaeili, K. & Harrisson, R. 2008. Observation of ore pass system performance at Brunswick mine. CIM Bulletin, **101**, 1-6.

[27] Hadjigeorgiou, J. & Lessard, J. 2007. Numerical investigations of ore pass hang-up phenomena. International Journal of Rock Mechanics and Mining Sciences, **44**, 820-834, doi: https://doi.org/10.1016/j.ijrmms.2006.12.006.

[28] Hadjigeorgiou, J. & Lessard, J. 2010. Strategies for restoring material flow in ore and waste pass systems. International Journal of Mining, Reclamation and Environment, **24**, 267-282.

[29] Hadjigeorgiou, J., Lessard, J.F. & Mercier-Langevin, F. 2005. Ore pass practice in Canadian mines. Journal of the Southern African Institute of Mining and Metallurgy, **105**, 809-816.

[30] Hadjigeorgiou, J. & Mercier-Langevin, F. 2008. Estimating ore pass longevity in hard rock mines. *The 42nd US Rock Mechanics Symposium (USRMS)*. American Rock Mechanics Association.

[31] Hadjigeorgiou, J. & Stacey, T.R. 2013. The absence of strategy in orepass planning, design, and management. Journal of the Southern African Institute of Mining and Metallurgy, **113**, 795-801.

[32] Hagan, T.O. & Acheampong, E. 1999. Current design, support and maintenance of rockpasses and assessment of practices applicable at depth. *Proceedings of the Second Southern African Rock Engineering Symposium*, Johannesburg, South Africa, 62-79.

[33] Hambley, D.F. 1987. Design of ore pass systems for underground mines. Canadian Institute of Mining (CIM) Bulletin, **897**, 25-30.

[34] Hambley, D.F., Pariseau, W.G. & Singh, M.M. 1983. *Guidelines for open pit ore pass design - Volume 1: Final Report.* U. S. Bureau of Mines Department of the Interior.

[35] Hambley, D.F. & Singh, M.M. 1983. *Guidelines for open pit ore pass design - Volume 2: Design Manual*. U. S. Bureau of Mines Department of the Interior.

[36] Joughin, W.C. & Stacey, T.R. 2004. The behaviour of ore passes in deep level tabular mines. *The 2nd International Seminar on Deep & High Stress Mining*. The Southern African Institute of Mining and Metallurgy (SAIMM), Johannesburg, South Africa, 395-411.

[37] Keen, A.J. & Udd, J.E. 1999. Mining in the Arctic. CRC Press, London.

[38]Kirsten, H.A.D. & Klokow, J.W. 1979. Control of fracturing in mine rock passes. *ISRM Congress*. ISRM, Montreux, Switzerland, 203-210.

[39] Koivisto, M. 2017. *Ore pass design and placement.* MSc European Mining Course - Aalto University

[40] Kvapil, R. 1982. The mechanics and design of sublevel caving systems. *In*: Hustrulid, W.A. (ed.) *Underground Mining Methods Handbook*. Society for Mining Metallurgy, United States, 880-897.

[41] Kvapil, R. 1998. Sub-level caving. *In*: Hartman, H.L. (ed.) *SME Mining Engineering Handbook*. Society for Mining, Metallurgy, and Exploration (SME), 1789 - 1814.

[42] Lessard, J. & Hadjigeorgiou, J. 2003. Design tools to minimize the occurrence of ore pass interlocking hang-ups in metal mines. *The 10th ISRM Congress*. International Society for Rock Mechanics and Rock Engineering - South African Institute of Mining and Metallurgy, Sandton, South Africa, 757-762.

[43] Manzoor, S., Gustafson, A. & Schunnesson, H. 2023. Dumping oversize rock fragments in orepasses: the impact on the production cycle of a sublevel caving operation. Mining Technology, 1-10, doi: https://doi.org/10.1080/25726668.2023.2215560.

[44] McCracken, A. & Stacey, T.R. 1989. Geotechnical risk assessment for large-diameter raise-bored shafts. Transactions of the Institution of Mining and Metallurgy, **98**, A145-A150.

[45] Microtrac. 2020. Particle shape characterization by image analysis. Microtrac, 20.

[46] Nazeri, H. 2001. *Development of a discrete element methodology for the simulation of gravity flow of ore in ore passes.* PhD, Colorado School of Mines.

[47] Olivares Brûlé, D.N. 2016. *Experimental characterization of the flowability of material in block/panel caving.* MSc, The University of Chile.

[48] Onederra, I. & Chitombo, G. 2007. Design methodology for underground ring blasting. Mining Technology, **116**, 180-195.

[49] Pariseau, W.G. 1966. *The gravity induced movement of materials in ore passes analyzed as a problem in Coulomb plasticity.* PhD, University of Minnesota.

[50] Peele, R. & Church, J.A. 1947. Mining engineers' handbook. John Wiley & Sons.

[51] Pons, M.-N. & Dodds, J. 2015. Chapter Fifteen - Particle Shape Characterization by Image Analysis. *In*: Tarleton, S. (ed.) *Progress in Filtration and Separation*. Academic Press, Oxford, 609-636.

[52] Salmi, E.F., Phan, T., Sellers, E.J. & Stacey, T.R. 2024a. Expert Elicitation for the Resilient Design and Optimisation of Ultra-long Ore Passes for Deep Mass Mining. Mining, Metallurgy & Exploration, doi: https://doi.org/10.1007/s42461-024-00979-3.

[53] Salmi, E.F., Phan, T., Sellers, E.J. & Stacey, T.R. 2024b. A review on the geotechnical design and optimisation of ultra-long ore passes for deep mass mining. Environmental Earth Sciences, **83**, 301, doi: https://doi.org/10.1007/s12665-024-11616-z.

[54] Sato, A. & Tang, H. 2020. Analysis of ore pass hang-ups in long vertical ore passes by 3-D DEM. International Journal of Mining Engineering and Mineral Processing, **9**, 1-11, doi: http://article.sapub.org/10.5923.j.mining.20200901.01.html.

[55] Silke, R. 2009. The operational history of mines in the Northwest Territories. Canada An Historical Research Project, 511.

[56] Silva, M. & Casali, A. 2015. Modelling SAG milling power and specific energy consumption including the feed percentage of intermediate size particles. Minerals Engineering, **70**, 156-161.

[57] Singh, K.H. 1973. Reinforcement of an ore pass system: a case history. *The 8th Canadian Rock Mechanics Symposium*, 231-249.

[58] Sofianos, A.I. 1996. Analysis and design of an underground hard rock voussoir beam roof. International Journal of Rock Mechanics and Mining Sciences & Geomechanics Abstracts, **33**, 153-166, doi: https://doi.org/10.1016/0148-9062(95)00052-6.

[59] Sredniawa, W., Skawina, B., Garcia, J.R. & Rapp, J. 2023. Analyzing degradation of ore pass walls in Kiirunavaara mine using scanning data. Frontiers in Built Environment, **9**, 1-8, doi: https://doi.org/10.3389/fbuil.2023.1250671.

[60] Stacey, T.R. & Swart, A.H. 1997. *Investigation into drawpoints, tips orepasses and chutes.* Safety in Mines Research Advisory Comittee (SIMRAC).

[61] Sun, H., Zhao, L., Wei, L., Jia, J. & Zhou, S. 2024. Numerical Study of the Influence of Multiple Parameters on Hang-ups: Insight From a Structural and Mechanical Characteristics Analysis. Rock mechanics and rock engineering, doi: https://doi.org/10.1007/s00603-024-03783-z.

[62] Szwedzicki, T. 2007. Formation and removal of hang-ups in ore passes. Mining Technology, **116**, 139-145, doi: https://doi.org/10.1179/174328607X191047.

[63] Torres, R.S., Encina, V.M. & Segura, C.O. 1981. Damp mineral and its effect on block caving with gravity transfer. *In*: Stewart, D.R. (ed.) *Design and Operation of Caving and Sublevel Stoping Mines*. Society of Mining Engineers of the American Institute of Mining, Metallurgical, and Petroleum Engineers (AIME) - OneMine, 251-282.

[64] Turcotte, P. 2004. *Modeling of Blockages in Ore Passes Using the Distinct Element Method (In French).* MSc Thesis, University of Laval.

[65] Van Heerden, D. 2004a. The use of Calcium Aluminate Cement in shotcrete. *Shotcrete: More Engineering Developments: Proceedings of the Second International Conference on Engineering Developments in Shotcrete*, 267-274.

[66] Van Heerden, D. 2004b. The use of cementitious linings to protect ore passes in the mining industry. *In*: Villaescusa, E. & Potvin, Y. (eds.) *Ground Support in Mining & Underground Construction*. CRC Press, 1084-1106.

[67] Van Heerden, D., Fryda, H. & Saucier, F. 2005. Elements for effective design of abrasion resistant concretes. Journal of the Southern African Institute of Mining and Metallurgy, **105**, 771-781.

[68] Vieira, F.M.C.C. & Durrheim, R.J. 2005. Design and support of rockpasses at ultra-deep levels. Journal of the Southern African Institute of Mining and Metallurgy, **105**, 783-794, doi: https://hdl.handle.net/10520/AJA0038223X_3031.

Anexo A

Table 6: Composition of different muck types considered in the second series of experiments

New Particle Types	Parent Particles							
	S1	S2	S3	S4	P1	P2	O1	I1
SS1	25%	25%	25%	25%				
SS2	50%	20%	20%	10%				
SS3	10%	20%	20%	50%				
SS4	20%	0%	0%	80%				
SS5	80%	0%	0%	20%				
SS6	50%	0%	0%	50%				
SS7	80%	20%	0%	0%				
SS8	20%	80%	0%	0%				
SS9	50%	50%	0%	0%				
SS10	80%	0%	20%	0%				
SS11	20%	0%	80%	0%				
SS12	50%	0%	50%	0%				
SS13	0%	80%	20%	0%				
SS14	0%	20%	80%	0%				
SS15	0%	50%	50%	0%				
SS16	0%	80%	0%	20%				
SS17	0%	20%	0%	80%				
SS18	0%	50%	0%	50%				
SS19	0%	0%	80%	20%				
SS20	0%	0%	20%	80%				
SS21	0%	0%	50%	50%				
PP1					20%	80%		
PP2					80%	20%		
PP3					50%	50%		
D1		25%				25%	25%	25%
D2		33%				33%	33%	
D3						33%	33%	33%
D4		33%					33%	33%
D5		33%				33%		33%
D6	50%				50%			
D7						50%		50%
D8		50%				50%		
D9							50%	50%
D10	50%						50%	
D11	50%							50%
D12					50%		50%	
D13					50%			50%
D14						50%	50%	
D15	25%				25%		25%	25%
D16	33%				33%		33%	
D17					33%		33%	33%
D18	33%						33%	33%
D19	33%					33%		33%
D20	50%					50%		

UNIVERSIDAD DE CONCEPCIÓN - FACULTAD DE INGENIERÍA

Departamento de Ingeniería Metalúrgica

Hoja Resumen Memoria de Título

Título: Experimental study of ore flow to assess the feasibility of using long ore passes for the decarbonization of hauling in deep mining operations	
Nombre Memorista: Fernanda Scarlet Vera Valverde	

Modalidad	**Proyecto**	**Profesor (es) Patrocinante (s)**
Concepto	EXCELENTE	
Calificación	6.9	
Fecha	19.12.2024	**Prof. René Gómez Puigpinos**
Prof. Ramón Díaz N.		**Ingeniero Supervisor: Dr. Ebrahim Fathi Salmi** **Institución:** Commonwealth Scientific and Industrial Research Organisation, Australia.

Comisión (Nombre y Firma)	
Prof. Roberto Fustos Toribio	**Dr. Ebrahim Fathi Salmi**

Resumen

La disminución continua en la ley de los minerales ha obligado a la industria minera a implementar nuevas estrategias para mantener e incluso aumentar la producción, especialmente debido a la creciente demanda de minerales estratégicos y críticos como el cobre, que es crucial para la transición energética. El cobre extraído de minas subterráneas mediante métodos de hundimiento frecuentemente emplea piques de traspaso, como un método de transporte del mineral entre niveles. El aumento en el uso y extensión de los piques de traspaso en la producción minera tiene el potencial de mejorar la eficiencia, reducir el consumo de energía y disminuir las emisiones de carbono, específicamente en el transporte de materiales. Sin embargo, existen desafíos significativos relacionados con el flujo gravitacional en los piques de traspaso debido a las grandes distancias verticales en estos métodos y a la mayor profundidad de las actividades mineras.

Para abordar estos desafíos, este estudio emplea un modelo físico a escala para examinar las características del flujo de diferentes tipos de partículas dentro de un pique de traspaso. Las variables analizadas incluyen diferentes porcentajes de llenado, distribuciones de tamaño de partículas y propiedades de las partículas. Se realizaron un total de 4160 experimentos de flujo, utilizando 52 combinaciones de formas y tamaños de partículas, para identificar y cuantificar el efecto de diferentes variables en el flujo del material.

En los resultados experimentales, el mayor número de colgaduras se registró para partículas prismáticas triangulares grandes, con un total de 125 atascos, seguidas por partículas esféricas grandes, con 96 atascos. En contraste, no se observaron atascos en experimentos con partículas esféricas pequeñas y partículas octaédricas. Además, el índice de frecuencia de atascos se reduce en un 98.48% cuando la esfericidad disminuye en un 23.47%. Esto indica que una disminución en la esfericidad tiene un impacto significativo en el flujo de partículas. En partículas esféricas, menores

niveles de llenado del pique de traspaso reducen el número de atascos; sin embargo, en partículas de forma prismática mixta, este efecto no se observó.

El análisis detallado de los eventos de atascos bajo diversas condiciones ayuda a identificar escenarios críticos de flujo de partículas dentro de los piques de traspaso. Los hallazgos proporcionan información invaluable sobre las condiciones críticas que afectan el flujo de partículas, mejorando así nuestra comprensión de la dinámica compleja en las operaciones de los piques de traspaso de mineral.